

# Analytic study of the effect of dark energy-dark matter interaction on the growth of structures

Rafael J. F. Marcondes,<sup>a</sup> Ricardo C. G. Landim,<sup>a</sup> André A. Costa,<sup>a</sup> Bin Wang<sup>b</sup> and Elcio Abdalla<sup>a</sup>

<sup>a</sup>Departamento de Física Matemática, Instituto de Física, Universidade de São Paulo, Rua do Matão 1371, São Paulo, Brazil

<sup>b</sup>Department of Physics and Astronomy, Shanghai Jiao Tong University 200240 Shanghai, China

E-mail: [rafaelmarcondes@usp.br](mailto:rafaelmarcondes@usp.br), [rlandim@if.usp.br](mailto:rlandim@if.usp.br), [alencar@if.usp.br](mailto:alencar@if.usp.br), [wang\\_b@sjtu.edu.cn](mailto:wang_b@sjtu.edu.cn), [eabdalla@if.usp.br](mailto:eabdalla@if.usp.br)

**Abstract.** Large-scale structure has been shown as a promising cosmic probe for distinguishing and constraining dark energy models. Using the growth index parametrization, we obtain an analytic formula for the growth rate of structures in a coupled dark energy model in which the exchange of energy-momentum is proportional to the dark energy density. We find that the evolution of  $f\sigma_8$  can be determined analytically once we know the coupling, the dark energy equation of state, the present value of the dark energy density parameter and the current mean amplitude of dark matter fluctuations. After correcting the growth function for the correspondence with the velocity field through the continuity equation in the interacting model, we use our analytic result to compare the model's predictions with large-scale structure observations.

**Keywords:** dark energy theory, cosmological parameters from LSS

**ArXiv ePrint:** [1605.05264](https://arxiv.org/abs/1605.05264)

---

## Contents

<b>1</b>	<b>Introduction</b>	<b>1</b>
<b>2</b>	<b>Cosmology with DE and DM interactions</b>	<b>2</b>
2.1	The background universe	3
2.2	The perturbed equations	3
2.3	The phenomenological coupled DE model and the DM evolution	5
<b>3</b>	<b>The analytical growth rate and amplitude of perturbations</b>	<b>5</b>
3.1	The growth of structure in the CDE model	6
3.2	Stability conditions	9
3.3	Comparison with full numerical computations in CAMB	10
<b>4</b>	<b>Observational constraints</b>	<b>11</b>
4.1	The data	12
4.2	The statistical method	14
4.3	The results	14
<b>5</b>	<b>Conclusions</b>	<b>21</b>
<b>A</b>	<b>The case of an interaction proportional to the DM density</b>	<b>22</b>

---

## 1 Introduction

Observations of Type Ia supernovae (SNe Ia) [1, 2] at the end of the 1990s culminated in the currently well established fact that the Universe is undergoing a phase of accelerated expansion. In the framework of General Relativity (GR), some exotic form of matter with negative pressure — the dark energy (DE) — or a simple positive cosmological constant ( $\Lambda$ ) can account for such acceleration.

Prior to the idea of DE is another unknown component referred to as dark matter (DM). At the level of galaxy structures, the amount of visible matter in galaxies is not large enough to explain the observed rotation curves, which differ from the prediction of classical mechanics when considering the gravitational field generated by the visible matter [3, 4]. A possible solution is the existence of a kind of matter that neither interacts with radiation nor with the conventional matter except through the gravitational field or through some feeble interaction.

The Universe turns out to be remarkably well described by a model composed mostly of these two dark components and smaller fractions of baryonic matter and radiation, the  $\Lambda$ -Cold Dark Matter ( $\Lambda$ CDM) model. This concordance  $\Lambda$ CDM model, with a phase of extremely fast expansion (dubbed inflation) right after the Big Bang, is widely accepted as the de facto model of the Universe. But still, it leaves some questions unanswered. One of them is the seeming coincidence that matter and dark energy are found to contribute to the energy content of the Universe with amounts of the same order today, despite behaving quite differently with respect to the expansion. Posed this way, this fact has been known as the cosmic coincidence problem. Some authors have proposed the existence of a mechanism that

drives the ratio between the two components close to 1 at late times. An interaction between the dark components would provide just that [5–7], while appearing to be compatible with observations. The possibility of such an interaction should be regarded as the natural case for these components, whose natures we do not know, rather than as a particular case of a bigger scenario. It could then be a solution or at least an alleviation to the coincidence problem.

Several authors have built and constrained interacting DE models with observations, mostly of SNe Ia, Cosmic Microwave Background (CMB), baryon acoustic oscillations (BAO), galaxy clusters and  $H(z)$  data [8–18]. For more comprehensive references, see the review ref. [19]. More recently, researchers have been also attempting to detect the effect of interaction on the clustering of matter, through the rate at which structures form, which can be measured with redshift-space distortions (RSDs) [20–24]. The fact that the interaction is expected to affect the growth of structures more than it affects phenomena from remote epochs, e.g. the CMB, makes this low-redshift observable particularly interesting. One can expect to see the imprint of the interaction on matter structures by analyzing the rate at which they grow compared to how the non-interacting standard cosmology predicts.

It is interesting that the evolution of the growth rate can be solved approximately in an analytic form,  $f(z) \approx [\Omega_M(z)]^{\gamma(z)}$ . The approximation was first proposed by Peebles [25] for the matter dominated universe as  $f(z=0) \approx (\Omega_{M,0})^{0.6}$ , followed by the more accurate approximation  $(\Omega_{M,0})^{4/7}$  by Lightman & Schechter [26]. More generally, the approximation was also obtained in dynamical DE models with zero curvature and slowly varying equation of state [27] and in curved spaces [28]. In modified gravity models, the approximate solution was given in refs. [29, 30]. Since growth data spans a wide range of redshift and the growth index evolves with the redshift, it is worth exploring its parametrization as a function of the redshift. This can help distinguish between DE models and modified gravity models [31, 32].

In this work we will investigate the influence of a DE-DM interaction on the growth of structures. Our main purpose is to solve analytically the growth rate of matter perturbations as a function of the redshift in an interacting DE model. We will generalize the method employed for the dynamical DE model without any interaction with DM in ref. [20]. Our derivation is based on the expansion of the growth index and of the DE equation of state (EoS) parameter in terms of the DE density parameter  $\Omega_{DE}(z)$ . We will also derive an expression for the root-mean-square (rms) amplitude of perturbations  $\sigma_8(z)$  and show that when the DE equation of state, the coupling, the DE energy density and the amplitude of perturbations at present are given, the evolution history of the growth of structures is fully determined analytically. This analytic solution of the growth can help us clearly see the influence of the interaction between dark sectors in the growth. With the analytic form of  $f\sigma_8(z)$  obtained, we can test the interacting DE model by using RSD observations.

The outline of this paper is as follows: in section 2 we introduce the phenomenological model. Section 3 goes deeply into the dynamical equations governing the perturbations of the fluids, according to GR. We then compare our model predictions with RSDs in section 4 and give our conclusions in section 5.

## 2 Cosmology with DE and DM interactions

Although some models inspired by Quantum Field Theory have been proposed [17, 33] attempting to explain the interaction between dark sectors at the Lagrangian level, here we will concentrate on the phenomenological approach to describe the interaction between DE and

DM. We represent the interaction by non-vanishing contributions to the right-hand side of the energy-momentum tensor conservation equations for the dark fluids, preserving, however, the total energy-momentum conservation.

## 2.1 The background universe

Hereafter we consider a universe described, at the background level, by the flat Friedmann-Lemaître-Robertson-Walker (FLRW) metric, which we write in terms of the conformal time  $\tau$ ,  $ds^2 = a^2(\tau) (-d\tau^2 + \delta_{ij} dx^i dx^j)$ , where  $a(\tau)$  is the scale factor and  $x^i$  are the spatial coordinates. We use latin letters  $i, j, \dots$  for the spatial indices 1, 2, 3 and greek letters  $\mu, \nu, \dots$  for the indices 0, 1, 2 and 3. Dots denote derivatives with respect to the conformal time.

We consider the universe composed only of dark matter and dark energy, with zero curvature. The components are treated as fluids, with energy-momentum tensor

$$\bar{T}_{\mu\nu} = \bar{p}\bar{g}_{\mu\nu} + (\bar{p} + \bar{\rho})\bar{u}_\mu\bar{u}_\nu, \quad (2.1)$$

where  $\bar{p}$  and  $\bar{\rho}$  are the pressure and energy density of the fluid,  $\bar{u}^\mu$  its four-velocity, and  $\bar{g}_{\mu\nu}$  the metric. The bars indicate that the quantities are unperturbed. In the standard model, the fluids satisfy the energy-momentum conservation  $\nabla_\mu \bar{T}^\mu{}_\nu = 0$ . An interaction is introduced by rewriting this equation as

$$\nabla_\mu \bar{T}^\mu{}_\nu{}^{\text{DM}} = \bar{Q}_\nu{}^{\text{DM}}, \quad (2.2a)$$

$$\nabla_\mu \bar{T}^\mu{}_\nu{}^{\text{DE}} = \bar{Q}_\nu{}^{\text{DE}}, \quad (2.2b)$$

for both fluids. Total energy-momentum conservation requires  $\bar{Q}_\nu{}^{\text{DE}} = -\bar{Q}_\nu{}^{\text{DM}}$ . As a result of the homogeneity and isotropy of the background, the spatial components of  $\bar{Q}_\nu$  are zero. The fluids are comoving with the Hubble flow, with  $\bar{u}^\mu = (a^{-1}, 0, 0, 0)$ . The unperturbed energy-momentum tensors of the two fluids have their non-zero components given by  $\bar{T}^0{}_0 = -\bar{\rho}$ ,  $\bar{T}^i{}_j = \bar{p}\delta^i_j$ . The  $\nu = 0$  energy-momentum conservation equation thus reads

$$\dot{\bar{\rho}} + 3\mathcal{H}(1+w)\bar{\rho} = a^2\bar{Q}^0 = -\bar{Q}_0, \quad (2.3)$$

for each of the two dark fluids, with  $\mathcal{H} \equiv \dot{a}/a$  and  $w \equiv \bar{p}/\bar{\rho}$  the equation of state (EoS) parameter. The background evolution of the universe as a whole is governed by the Friedmann equation, from the unperturbed time-time Einstein's field equation (EFE),

$$\mathcal{H}^2 = \frac{8\pi G}{3} a^2 (\bar{\rho}_{\text{DM}} + \bar{\rho}_{\text{DE}}). \quad (2.4)$$

## 2.2 The perturbed equations

We consider scalar perturbations only. Since we intend to discuss the gravitational evolution of perturbations, it is more convenient to work in the conformal (Newtonian) gauge. Scalar perturbations develop at low redshifts in the era of structure formation. In the conformal gauge, the line element is written as

$$ds^2 = a^2(\tau) [-(1+2\psi)d\tau^2 + (1-2\phi)\delta_{ij}dx^i dx^j], \quad (2.5)$$

with  $\phi = \phi(x^\mu)$  and  $\psi = \psi(x^\mu)$  being small perturbations, satisfying  $|\phi|, |\psi| \ll 1$ . The metric is given by

$$g_{00} = -a^2(1+2\psi), \quad g_{0i} = g_{i0} = 0, \quad g_{ij} = a^2(1-2\phi)\delta_{ij}. \quad (2.6)$$

Assuming that there is no anisotropic stress, we have  $\psi = \phi$ . We rewrite the metric separating its unperturbed part and the perturbation  $h_{\mu\nu}$  as  $g_{\mu\nu} = \bar{g}_{\mu\nu} + h_{\mu\nu}$ . We have then  $\bar{g}_{00} = -a^2$ ,  $\bar{g}_{ij} = a^2\delta_{ij}$ ,  $h_{00} = -2a^2\phi$ ,  $h_{ij} = -2a^2\phi\delta_{ij}$ . The unperturbed metric  $\bar{g}$  must be used to lower or raise indices of unperturbed tensors. We denote the perturbed parts of all other quantities by their own symbol preceded by a  $\delta$ , as in  $B \equiv \bar{B} + \delta B$ . The perturbations must satisfy  $|\delta B| \ll |\bar{B}|$ .

The components of the perturbed energy-momentum tensors, from perturbing eq. (2.1), are

$$\begin{aligned}\delta T^0_0 &= -\delta\rho, & \delta T^i_j &= \delta p \delta^i_j, & \delta T_{00} &= a^2(\delta\rho + 2\bar{\rho}\phi), \\ \delta T^i_0 &= -a^{-1}(\bar{\rho} + \bar{p})\delta u^i, & \delta T^0_i &= a^{-1}(\bar{\rho} + \bar{p})\delta u_i, & & \\ \delta T_{0i} &= \delta T_{i0} = -a(\bar{\rho} + \bar{p})\delta u_i, & \delta T_{ij} &= a^2(\delta p - 2\bar{p}\phi)\delta_{ij}.\end{aligned}\quad (2.7)$$

With these perturbed metric and energy-momentum tensor, the perturbed conservation equations give the following evolution equations for the perturbations,

$$-\dot{\delta} - \left[ 3\mathcal{H}(c_s^2 - w) - \frac{\bar{Q}_0}{\bar{\rho}} \right] \delta - (1+w)(\theta - 3\dot{\phi}) = \frac{\delta Q_0}{\bar{\rho}}, \quad (2.8a)$$

$$\dot{\theta} + \left[ \mathcal{H}(1-3w) - \frac{\bar{Q}_0}{\bar{\rho}} + \frac{\dot{w}}{1+w} \right] \theta - k^2\phi - \frac{c_s^2}{1+w}k^2\delta = \frac{ik^i\delta Q_i}{\bar{\rho}(1+w)}, \quad (2.8b)$$

where we have introduced the relative density perturbation  $\delta \equiv \delta\rho/\bar{\rho}$  and used  $\delta u_0 = -a\phi$ , from the condition  $g_{\mu\nu}u^\mu u^\nu = -1$ .  $\delta Q_\mu$  are the perturbations to the exchange of energy-momentum in the perturbed conservation equations,  $c_s^2 \equiv \delta p/\delta\rho$  is the sound speed of the fluid,  $k^i$  are the components of the wavevector in Fourier space, and  $\theta \equiv a^{-1}ik^j\delta u_j$  is the divergence of the velocity perturbation in Fourier space.

The perturbed time-time EFE is the Poisson equation, relating  $\phi$  and the total density perturbation of the fluids. The full Poisson equation in Fourier space is

$$(1 + 3\mathcal{H}^2/k^2)k^2\phi = -3\mathcal{H}\dot{\phi} - 4\pi G a^2(\bar{\rho}_{\text{DM}}\delta_{\text{DM}} + \bar{\rho}_{\text{DE}}\delta_{\text{DE}}). \quad (2.9)$$

In order to analyze the growth of structures, we need to combine equations (2.8) with the Poisson equation to substitute  $\phi$  in terms of  $\delta_{\text{DM}}$ . Since structures grow in the Newtonian regime, on spatial scales much smaller than the horizon ( $k \gg \mathcal{H}$ ) and with negligible time variation of the potential, we can discard the second term in the left-hand side of eq. (2.9) and the term proportional to  $\dot{\phi}$ . Also, the dark energy perturbations are expected to be negligible on sub-horizon scales [34]. The Poisson equation then reduces to

$$k^2\phi = -4\pi G a^2 \bar{\rho}_{\text{DM}} \delta_{\text{DM}} = -\frac{3}{2}\mathcal{H}^2 \Omega_{\text{DM}} \delta_{\text{DM}}, \quad (2.10)$$

the last equality coming from eq. (2.4) with the density parameter of the DM fluid defined as  $\Omega_{\text{DM}} \equiv \bar{\rho}_{\text{DM}}/\bar{\rho}_{\text{critical}}$ , the critical density being equal to the total density  $\bar{\rho}_{\text{total}} = \bar{\rho}_{\text{DM}} + \bar{\rho}_{\text{DE}}$  (and thus  $\Omega_{\text{DE}} = 1 - \Omega_{\text{DM}}$ ) in the absence of curvature. Finally, combining equations (2.8) and (2.10) together, we get the second order differential equation for the DM perturbation

$$\ddot{\delta}_{\text{DM}} - (\mathcal{Q} - \mathcal{K})\dot{\delta}_{\text{DM}} - \left( \frac{3}{2}\mathcal{H}^2\Omega_{\text{DM}} + \dot{\mathcal{Q}} + \mathcal{K}\mathcal{Q} \right) \delta_{\text{DM}} = -\frac{ik^i\delta Q_i^{\text{DM}}}{\bar{\rho}_{\text{DM}}}, \quad (2.11)$$

with

$$\mathcal{Q} \equiv \frac{\bar{Q}_0^{\text{DM}}}{\bar{\rho}_{\text{DM}}} - \frac{\delta Q_0^{\text{DM}}}{\bar{\rho}_{\text{DM}}\delta_{\text{DM}}} \quad \text{and} \quad \mathcal{K} \equiv \mathcal{H} - \frac{\dot{\bar{Q}}_0^{\text{DM}}}{\bar{\rho}_{\text{DM}}}. \quad (2.12)$$

Eq. (2.11) is general and valid for any type of interaction. In the next subsection we simplify this equation by choosing a particular coupled model.

### 2.3 The phenomenological coupled DE model and the DM evolution

We analyze a model with an interaction term in the DM energy-momentum conservation equation that is proportional to the DE energy density,

$$\text{CDE:} \quad Q_0^{\text{DM}} = \bar{Q}_0^{\text{DM}} = -3\mathcal{H}\xi\bar{\rho}_{\text{DE}}. \quad (2.13)$$

Models like this, with interaction proportional to  $\rho_{\text{DE}}$ ,  $\rho_{\text{DM}}$  or their combination, have been extensively studied in the last years, for example in refs. [9–12, 15, 16] (see also the recent review [19]). The interaction in this coupled dark energy (CDE) model has only an unperturbed part, since we are neglecting DE clustering. With eq. (2.13), the background evolution eq. (2.3) reads

$$\dot{\bar{\rho}}_{\text{DM}} + 3\mathcal{H}\bar{\rho}_{\text{DM}} = 3\mathcal{H}\xi\bar{\rho}_{\text{DM}}\frac{1-\Omega_{\text{DM}}}{\Omega_{\text{DM}}}. \quad (2.14)$$

Replacing  $\frac{\bar{Q}_0^{\text{DM}}}{\bar{\rho}_{\text{DM}}} = -3\mathcal{H}\xi\frac{1-\Omega_{\text{DM}}}{\Omega_{\text{DM}}}$  and  $\frac{\delta Q_0^{\text{DM}}}{\bar{\rho}_{\text{DM}}\delta_{\text{DM}}} = 0$ , eqs. (2.8) for DM are

$$\dot{\delta}_{\text{DM}} + 3\mathcal{H}\xi\frac{1-\Omega_{\text{DM}}}{\Omega_{\text{DM}}}\delta_{\text{DM}} + \theta_{\text{DM}} = 0, \quad (2.15a)$$

$$\dot{\theta}_{\text{DM}} + \mathcal{H}\left(1 + 3\xi\frac{1-\Omega_{\text{DM}}}{\Omega_{\text{DM}}}\right)\theta_{\text{DM}} + \frac{3}{2}\mathcal{H}^2\Omega_{\text{DM}}\delta_{\text{DM}} = 0, \quad (2.15b)$$

and the evolution of the DM perturbations (2.11) reduces to

$$\ddot{\delta}_{\text{DM}} + \left(1 + 6\xi\frac{1-\Omega_{\text{DM}}}{\Omega_{\text{DM}}}\right)\mathcal{H}\dot{\delta}_{\text{DM}} - \frac{3}{2}\mathcal{H}^2\delta_{\text{DM}}\left[\Omega_{\text{DM}} - 2\xi\frac{1-\Omega_{\text{DM}}}{\Omega_{\text{DM}}}\left(1 + \frac{\dot{\mathcal{H}}}{\mathcal{H}^2} + 3\xi\frac{1-\Omega_{\text{DM}}}{\Omega_{\text{DM}}} - \frac{\dot{\Omega}_{\text{DM}}}{\mathcal{H}\Omega_{\text{DM}}}\frac{1}{1-\Omega_{\text{DM}}}\right)\right] = 0. \quad (2.16)$$

The standard evolution  $\ddot{\delta}_{\text{DM}} + \mathcal{H}\dot{\delta}_{\text{DM}} - \frac{3}{2}\mathcal{H}^2\Omega_{\text{DM}}\delta_{\text{DM}} = 0$  is recovered when  $\xi = 0$ . Due to the presence of the interaction, the coefficient of  $\delta_{\text{DM}}$  in eq. (2.16) can become positive as  $\Omega_{\text{DM}}$  decreases, leading to a decaying regime of the perturbation. This negative growth rate, as we will see in section 3, cannot be described by the parametrization of  $f$  with the growth index.

### 3 The analytical growth rate and amplitude of perturbations

The growth rate  $f$  is defined as the logarithmic derivative of the (total) matter perturbation with respect to the logarithm of the scale factor,

$$f \equiv \frac{d \ln \delta_{\text{M}}}{d \ln a}, \quad (3.1)$$

and is often parametrized by

$$f \approx \Omega_{\text{M}}^\gamma. \quad (3.2)$$

The exponent  $\gamma$  is called the growth index. This approximation has been shown very satisfactory until now for virtually any cosmological model without DE-DM coupling, with  $\gamma$  varying accordingly (see, for example, ref. [35] and references therein). In the  $\Lambda$ CDM model, the growth index is approximately 6/11.

One can explore  $\gamma$  in different models by expanding it in terms of the DE density parameter. This can then be used to test and compare models since we can measure the growth rate as a function of the redshift.

### 3.1 The growth of structure in the CDE model

To obtain the approximation  $f \approx \Omega_{\text{DM}}^\gamma$ , we need to change the time derivatives  $\partial/\partial\tau$  to  $\partial/\partial a$  and write eq. (2.16) in terms of  $f$ . We can carry out the Taylor expansion for the functions in terms of  $\Omega_{\text{DE}}$  around zero, describing the time evolution in terms of the DE density abundance. In non-interacting models, a polynomial equation in  $\Omega_{\text{DE}}$  can be obtained by equating coefficients in both sides, with its zero-th order coefficients vanishing identically and its coefficients for higher orders in  $\Omega_{\text{DE}}$  giving the coefficients of  $\gamma = \sum_{n=0}^{\infty} \gamma_n (\Omega_{\text{DE}})^n$  in terms of the coefficients of  $w_{\text{DE}} = \sum_{n=0}^{\infty} w_n (\Omega_{\text{DE}})^n$  (see, for example, ref. [27]). This form of parametrization has been shown useful in obtaining the analytic expression of the growth index in dynamical DE models and convenient for distinguishing the model from the  $\Lambda$ CDM model [20, 27].

For the DE-DM interaction model, we will adopt the same strategy as that of the non-interacting cases [20]. We will do the expansion around  $\Omega_{\text{DE}} = 0$  and assume that the ratio between the rate of change of the DE density parameter and the Hubble rate is negligible compared to the density parameter and to unity, at least in the regime of structure formation. Therefore,  $\dot{\Omega}_{\text{DE}}/\mathcal{H} \ll \Omega_{\text{DE}}$  in eq. (2.16) and we are led to

$$\begin{aligned} \ddot{\delta}_{\text{DM}} + \left(1 + 6\xi \frac{1-\Omega_{\text{DM}}}{\Omega_{\text{DM}}}\right) \mathcal{H} \dot{\delta}_{\text{DM}} - \\ - \frac{3}{2} \mathcal{H}^2 \delta_{\text{DM}} \left\{ \Omega_{\text{DM}} + 2\xi \frac{1-\Omega_{\text{DM}}}{\Omega_{\text{DM}}} \left[-\frac{1}{2} + 3w_{\text{DE}}(1-\Omega_{\text{DM}}) - 3\xi \frac{1-\Omega_{\text{DM}}}{\Omega_{\text{DM}}}\right] \right\} = 0. \end{aligned} \quad (3.3)$$

After some manipulations, this is rewritten as

$$\begin{aligned} \frac{d^2 \ln \delta_{\text{DM}}}{d \ln a^2} + \left(\frac{d \ln \delta_{\text{DM}}}{d \ln a}\right)^2 + \left[\frac{1}{2} - \frac{3}{2} w_{\text{DE}} (1 - \Omega_{\text{DM}}) + 6\xi \frac{1 - \Omega_{\text{DM}}}{\Omega_{\text{DM}}}\right] \frac{d \ln \delta_{\text{DM}}}{d \ln a} - \\ - \frac{3}{2} \Omega_{\text{DM}} + 3\xi \frac{1 - \Omega_{\text{DM}}}{\Omega_{\text{DM}}} \left[\frac{1 - \Omega_{\text{DM}}}{\Omega_{\text{DM}}} (3\xi - 3w_{\text{DE}} \Omega_{\text{DM}}) + \frac{1}{2}\right] = 0. \end{aligned} \quad (3.4)$$

Substituting  $f$ , we have

$$\begin{aligned} \frac{df}{d \ln a} + f^2 + f \left[\frac{1}{2} - \frac{3}{2} w_{\text{DE}} (1 - \Omega_{\text{DM}}) + 6\xi \frac{1 - \Omega_{\text{DM}}}{\Omega_{\text{DM}}}\right] - \frac{3}{2} \Omega_{\text{DM}} + \\ + 3\xi \frac{1 - \Omega_{\text{DM}}}{\Omega_{\text{DM}}} \left[\frac{1 - \Omega_{\text{DM}}}{\Omega_{\text{DM}}} (3\xi - 3w_{\text{DE}} \Omega_{\text{DM}}) + \frac{1}{2}\right] = 0, \end{aligned} \quad (3.5)$$

which still has the first term parametrized by the scale factor. Next, we write  $\frac{df}{d \ln a} = \frac{d\Omega_{\text{DM}}}{d \ln a} \frac{df}{d\Omega_{\text{DM}}}$  and use the (background) energy conservation equations to substitute  $\frac{d\Omega_{\text{DM}}}{d \ln a}$ . The

total conservation equation gives

$$\begin{aligned}
d\bar{\rho}_{\text{total}} + 3\frac{da}{a}(\bar{\rho}_{\text{total}} + \bar{p}_{\text{total}}) &= 0, \\
d(a^3\bar{\rho}_{\text{total}}) &= -d(a^3)w_{\text{DE}}\bar{\rho}_{\text{DE}}, \\
d\left(\frac{a^3\bar{\rho}_{\text{DM}}}{\Omega_{\text{DM}}}\right) &= -d(a^3)w_{\text{DE}}\bar{\rho}_{\text{DM}}\frac{1-\Omega_{\text{DM}}}{\Omega_{\text{DM}}},
\end{aligned} \tag{3.6}$$

where we have used  $\bar{\rho}_{\text{total}} = \frac{\bar{\rho}_{\text{DM}}}{\Omega_{\text{DM}}}$  and  $\bar{\rho}_{\text{DE}} = \bar{\rho}_{\text{DM}}\frac{1-\Omega_{\text{DM}}}{\Omega_{\text{DM}}}$ , while the DM equation gives

$$\begin{aligned}
d\bar{\rho}_{\text{DM}} + 3\frac{da}{a}\bar{\rho}_{\text{DM}} &= 3\frac{da}{a}\xi\bar{\rho}_{\text{DM}}\frac{1-\Omega_{\text{DM}}}{\Omega_{\text{DM}}}, \\
d(a^3\bar{\rho}_{\text{DM}}) &= \xi\bar{\rho}_{\text{DM}}\frac{1-\Omega_{\text{DM}}}{\Omega_{\text{DM}}}d(a^3),
\end{aligned} \tag{3.7}$$

which can be inserted back in eq. (3.6) to give

$$\begin{aligned}
\xi\bar{\rho}_{\text{DM}}\frac{1-\Omega_{\text{DM}}}{\Omega_{\text{DM}}}\frac{d(a^3)}{\Omega_{\text{DM}}} - a^3\bar{\rho}_{\text{DM}}\frac{d\Omega_{\text{DM}}}{\Omega_{\text{DM}}^2} &= -w_{\text{DE}}\bar{\rho}_{\text{DM}}\frac{1-\Omega_{\text{DM}}}{\Omega_{\text{DM}}}d(a^3), \\
3\xi(1-\Omega_{\text{DM}})d\ln a - d\Omega_{\text{DM}} &= -3w_{\text{DE}}\Omega_{\text{DM}}(1-\Omega_{\text{DM}})d\ln a, \\
\frac{d\Omega_{\text{DM}}}{d\ln a} &= 3(1-\Omega_{\text{DM}})(\xi + w_{\text{DE}}\Omega_{\text{DM}}).
\end{aligned} \tag{3.8}$$

Substituting eq. (3.8) into  $\frac{df}{d\ln a} = \frac{d\Omega_{\text{DM}}}{d\ln a}\frac{df}{d\Omega_{\text{DM}}}$  and dividing eq. (3.5) by  $f$  we have

$$\begin{aligned}
3(\xi + w_{\text{DE}}\Omega_{\text{DM}})\frac{1-\Omega_{\text{DM}}}{f}\frac{df}{d\Omega_{\text{DM}}} + f + \frac{1}{2} - \frac{3}{2}w_{\text{DE}}(1-\Omega_{\text{DM}}) + 6\xi\frac{1-\Omega_{\text{DM}}}{\Omega_{\text{DM}}} - \frac{3}{2}\frac{\Omega_{\text{DM}}}{f} + \\
+ 3\xi\frac{1-\Omega_{\text{DM}}}{f\Omega_{\text{DM}}}\left[\frac{1-\Omega_{\text{DM}}}{\Omega_{\text{DM}}}(3\xi - 3w_{\text{DE}}\Omega_{\text{DM}}) + \frac{1}{2}\right] &= 0.
\end{aligned} \tag{3.9}$$

Finally, expanding eq. (3.9) around  $\Omega_{\text{DE}} = 0$  with  $f = (\Omega_{\text{DM}})^{\gamma_0 + \gamma_1\Omega_{\text{DE}} + \dots}$ , we arrive at the polynomial equation

$$\begin{aligned}
[3(1-w_0+5\xi) - \gamma_0(5-6w_0-6\xi)]\Omega_{\text{DE}} + \frac{1}{2}[-\gamma_0^2 + \gamma_0(1+12w_1+18\xi) - \\
- 2\gamma_1(5-12w_0-12\xi) - 6w_1 + 6\xi(5-6w_0+6\xi)]\Omega_{\text{DE}}^2 + \mathcal{O}(\Omega_{\text{DE}}^3) &= 0.
\end{aligned} \tag{3.10}$$

The zero-th order part is still identically zero even with non-zero  $\xi$ . The equations of the higher order terms can be solved to give the modified growth index coefficients

$$\gamma_0 = \frac{3(1-w_0+5\xi)}{5-6w_0-6\xi}, \tag{3.11a}$$

$$\gamma_1 = \frac{-\gamma_0^2 + \gamma_0(1+12w_1+18\xi) - 6w_1 + 6\xi(5-6w_0+6\xi)}{2(5-12w_0-12\xi)}, \tag{3.11b}$$

⋮

Eqs. (3.11) allow us to analyze the effect of the interaction and of the EoS on the growth index. We note that positive  $\xi$  increases  $\gamma_0$ , the dominant part of the growth index. For example, a  $\xi = \pm 0.01$  coupling changes  $\gamma_0$  by approximately  $\pm 3\%$  and the measured growth by up to  $\pm 9\%$  at  $z = 0$  when  $w_0 = -1$  and  $\sigma_{8,0}$  and  $\Omega_{\text{DE},0}$  are also fixed at fiducial  $\Lambda\text{CDM}$



values (see also figure 3). The well-known result  $\gamma_0 = \frac{3(1-w_0)}{5-6w_0}$  is recovered when  $\xi = 0$ , giving  $\gamma_0 = 6/11$  for  $\Lambda$ CDM. With the standard values  $w_0 = -1$  and  $\xi = 0$ , the first-order coefficient is  $\gamma_1 = \frac{3(5+11w_1)}{2057}$ , which gives a rather small contribution  $\gamma_1 \Omega_{\text{DE}}$  to  $\gamma$  for a slowly varying EoS parameter.

Predictions made with  $f = (\Omega_{\text{DM}})^{\gamma_0 + \gamma_1 \Omega_{\text{DE}} + \dots}$  can, in principle, be compared to growth rate measurements like those compiled in ref. [32]. Those data, however, are generally obtained from measurements of the RSD parameter  $\beta = f/b$ , where  $b$  is the bias measuring how galaxies trace the matter density field, and thus can be bias-dependent. Usually, it is preferable to compare predictions with the bias-independent data of the combination  $f\sigma_8$  [36], the growth rate multiplied by the variance of the density field filtered at a scale  $R = 8 h^{-1}$  Mpc, defined as

$$\sigma_R^2(z) \equiv \frac{1}{2\pi^2} \int_0^\infty dk k^2 P(k, z) |W(kR)|^2, \quad (3.12)$$

where  $P(k, z)$  is the matter power spectrum and  $W(kR)$  is the window function of the experiment in Fourier space. We derive  $\sigma_8$  from  $\delta_{\text{DM}}$  starting with the definition of  $f$ ,

$$\begin{aligned} \frac{d\Omega_{\text{DM}}}{d \ln a} \frac{d \ln \delta_{\text{DM}}}{d \Omega_{\text{DM}}} = (\Omega_{\text{DM}})^\gamma &\Rightarrow 3(1 - \Omega_{\text{DM}}) (\xi + w_{\text{DE}} \Omega_{\text{DM}}) \frac{d \ln \delta_{\text{DM}}}{d \Omega_{\text{DM}}} = (\Omega_{\text{DM}})^\gamma \quad \therefore \\ \therefore \frac{d \ln \delta_{\text{DM}}}{d \Omega_{\text{DE}}} &= -\frac{(1 - \Omega_{\text{DE}})^\gamma}{3\Omega_{\text{DE}} [\xi + w_{\text{DE}} (1 - \Omega_{\text{DE}})]}. \end{aligned} \quad (3.13)$$

We integrate backwards in  $\Omega_{\text{DE}}$  from  $\Omega_{\text{DE},0}$  to  $\Omega_{\text{DE}}(z)$  and expand it to obtain

$$\begin{aligned} \ln \frac{\delta_{\text{DM}}}{\delta_{\text{DM},0}} &= \ln \left( \frac{\Omega_{\text{DE}}}{\Omega_{\text{DE},0}} \right)^{-1/3\tilde{w}_0} + \frac{\gamma_0 - \bar{\omega}_{01}}{3\tilde{w}_0} (\Omega_{\text{DE}} - \Omega_{\text{DE},0}) - \\ &- \frac{1}{6\tilde{w}_0} \left[ \frac{\gamma_0^2}{2} - \gamma_0 \left( \frac{1}{2} + \bar{\omega}_{01} \right) - \gamma_1 + \frac{1}{\tilde{w}_0} \left( w_0 \bar{\omega}_{01} - w_2 + \frac{w_1 \tilde{w}_1}{\tilde{w}_0} \right) \right] (\Omega_{\text{DE}}^2 - \Omega_{\text{DE},0}^2) + \\ &+ \mathcal{O}(\Omega_{\text{DE}}^3) + \mathcal{O}(\Omega_{\text{DE},0}^3) \end{aligned} \quad (3.14)$$

where we have introduced the definitions

$$\tilde{w}_n \equiv w_n + \xi \quad \text{and} \quad \bar{\omega}_{01} \equiv \frac{w_0 - w_1}{\tilde{w}_0}. \quad (3.15)$$

The time dependence of  $\delta_{\text{DM}}$  is parametrized by  $\Omega_{\text{DE}}$ .  $\delta_{\text{DM},0}$  and  $\Omega_{\text{DE},0}$  represent their values today. Eq. (3.14) then gives

$$\delta_{\text{DM}}(z) = \delta_{\text{DM},0} \mathcal{D}(z; 0), \quad \text{with} \quad \mathcal{D}(z; 0) \equiv \left[ \frac{\Omega_{\text{DE}}(z)}{\Omega_{\text{DE},0}} \right]^{-1/3\tilde{w}_0} \exp \left[ \frac{\varepsilon_1 \Delta_{\text{DE}}^{(1)} + \varepsilon_2 \Delta_{\text{DE}}^{(2)}}{3\tilde{w}_0} \right] \quad (3.16)$$

up to the second order in  $\Omega_{\text{DE}}$  and  $\Omega_{\text{DE},0}$ , with

$$\varepsilon_1 \equiv \gamma_0 - \bar{\omega}_{01}, \quad (3.17)$$

$$\varepsilon_2 \equiv -\frac{\gamma_0^2}{4} + \frac{\gamma_0}{2} \left( \frac{1}{2} + \bar{\omega}_{01} \right) + \frac{\gamma_1}{2} - \frac{1}{2\tilde{w}_0} \left( w_0 \bar{\omega}_{01} - w_2 + \frac{w_1 \tilde{w}_1}{\tilde{w}_0} \right), \quad (3.18)$$

$$\Delta_{\text{DE}}^{(n)} \equiv \Omega_{\text{DE}}^n(z) - \Omega_{\text{DE},0}^n. \quad (3.19)$$

$\mathcal{D}(z; 0)$  is the backward propagation function for the evolution of the DM perturbation from redshift zero to  $z$ . Noting that  $P(k, z) = [\mathcal{D}(z; 0)]^2 P_0(k)$  and  $\mathcal{D}$  is scale-independent, it follows directly from the definition (3.12) that  $\sigma_R^2 = \mathcal{D}^2 \sigma_{R,0}^2$ , i.e.,  $\sigma_R$  satisfies the same equation (3.16) for  $\delta_{\text{DM}}$ . Thus, at the scale  $R = 8 h^{-1} \text{Mpc}$ , we have

$$\sigma_8(z) = \sigma_{8,0} \left[ \frac{\Omega_{\text{DE}}(z)}{\Omega_{\text{DE},0}} \right]^{-1/3\tilde{w}_0} \exp \left[ \frac{\varepsilon_1 \Delta_{\text{DE}}^{(1)} + \varepsilon_2 \Delta_{\text{DE}}^{(2)}}{3\tilde{w}_0} \right], \quad (3.20)$$

also up to the second order in  $\Omega_{\text{DE}}$  and  $\Omega_{\text{DE},0}$ . Note that there can be some inaccuracy in the computation of  $\sigma_8(z)$  from eq. (3.20), since we are integrating a function that has been expanded around  $\Omega_{\text{DE}} = 0$  from redshift zero, where  $\Omega_{\text{DE}}$  is not so small, until  $z$ . This has the consequence of the errors of the expansion at low redshifts being accumulated for  $\sigma_8$  at any redshift and constitutes a limitation of the method. We also note that if  $|w_1|$  or  $|w_2|$  is too large, it is possible that they can make the exponential in eq. (3.20) grow enormously.

For the evaluation of  $\Omega_{\text{DE}}(z)$ , we have to use a recursive relation. The DM and DE densities, in terms of the redshift, are

$$\bar{\rho}_{\text{DM}}(z) = \bar{\rho}_{\text{DM},0} \exp \left[ \int_0^z \frac{3}{1+\tilde{z}} \left( 1 - \xi \frac{\Omega_{\text{DE}}}{1 - \Omega_{\text{DE}}} \right) d\tilde{z} \right], \quad (3.21a)$$

$$\bar{\rho}_{\text{DE}}(z) = \bar{\rho}_{\text{DE},0} \exp \left[ \int_0^z \frac{3}{1+\tilde{z}} [1 + w_{\text{DE}}(\tilde{z}) + \xi] d\tilde{z} \right]. \quad (3.21b)$$

The zero-th order DE density parameter is obtained by setting  $w_{\text{DE}} = w_0$  and neglecting the term  $\xi \frac{\Omega_{\text{DE}}}{1 - \Omega_{\text{DE}}} \approx \xi \Omega_{\text{DE}} + \xi \Omega_{\text{DE}}^2$ ,

$$\Omega_{\text{DE}}^{(0)} = \frac{\bar{\rho}_{\text{DE}}^{(0)}}{\bar{\rho}_{\text{DE}}^{(0)} + \bar{\rho}_{\text{DM}}^{(0)}} = \frac{\Omega_{\text{DE},0} (1+z)^{3\tilde{w}_0}}{1 - \Omega_{\text{DE},0} + \Omega_{\text{DE},0} (1+z)^{3\tilde{w}_0}}. \quad (3.22)$$

Now the density parameter up to the first order is calculated by using  $w_{\text{DE}} = w_0 + w_1 \Omega_{\text{DE}}^{(0)}$  and  $\xi \frac{\Omega_{\text{DE}}}{1 - \Omega_{\text{DE}}} = \xi \Omega_{\text{DE}}^{(0)}$ ,

$$\Omega_{\text{DE}}^{(1)}(z) = \frac{\Omega_{\text{DE},0} (1+z)^{3\tilde{w}_0} \left[ 1 - \Omega_{\text{DE},0} + \Omega_{\text{DE},0} (1+z)^{3\tilde{w}_0} \right]^{\tilde{w}_1/\tilde{w}_0}}{1 - \Omega_{\text{DE},0} + \Omega_{\text{DE},0} (1+z)^{3\tilde{w}_0} \left[ 1 - \Omega_{\text{DE},0} + \Omega_{\text{DE},0} (1+z)^{3\tilde{w}_0} \right]^{\tilde{w}_1/\tilde{w}_0}} \quad (3.23)$$

With equations (3.11), (3.20) and (3.23) we are now able to compute  $f(z)$  and  $\sigma_8(z)$  provided that we know the parameters  $\xi$ ,  $w_n$ , and  $\Omega_{\text{DE},0}$ . Once we know the coupling, DE EoS coefficients, DE density parameter and the mean perturbation amplitude at present we can determine analytically how structures have evolved and can compare these results with large-scale structure (LSS) observations.

### 3.2 Stability conditions

Interacting DE models with constant EoS have already been shown to suffer from instabilities with respect to curvature and dark energy perturbations [37, 38]. Depending on some combinations of the sign of the interaction and on the dark energy being of the quintessence or phantom type,  $\delta_{\text{DE}}$  and the potential  $\phi$  can blow up. Table 1 summarizes the allowed regions for the interaction and the DE equation of state parameters in the CDE model as

**Table 1:** Stability conditions of the CDE model.

Constant EoS	Interaction sign	Condition
$w_{\text{DE}} < -1$	$\xi < 0$	early-time instability
$w_{\text{DE}} < -1$	$\xi > 0$	stable
$-1 < w_{\text{DE}} < 0$	$\xi < 0$	stable
$-1 < w_{\text{DE}} < 0$	$\xi > 0$	early-time instability

shown by ref. [39], which extends the model stability analysis of ref. [38] to negative values of  $\xi$ .

These results strongly restrict the parameter space for interacting DE. As those references point out, such instabilities can be avoided by allowing the EoS to vary with time, which we do when we expand  $w_{\text{DE}}$  in terms of  $\Omega_{\text{DE}}$ . However, before considering a time variable EoS, first we simplify our models by fixing  $w_1$  so we have one less parameter to be constrained with the Markov Chain Monte Carlo (MCMC) method. We proceed in the next section to compare our results for the growth rate with numerical calculations provided by a modified version of **CAMB** [40], in order to assess the reliability of our expressions and validate the method.

### 3.3 Comparison with full numerical computations in **CAMB**

To test how effective our analytical result of the growth in the CDE model is, we compare it with the numerical  $f(z)$  obtained in a modified version of **CAMB** for the interacting model.<sup>1</sup> We are going to show that our analytic solution can be trusted and we can further use it to estimate the cosmological parameters with a MCMC code, as a shortcut alternative to the full numerical computation to speed up the calculation.

We fix  $w_1 = 0$  and  $\Omega_{\text{DE},0} = 0.7$  and calculate  $f(z)$  with  $z$  ranging from 0 to 10. According to the stability conditions given in the last section, the interaction constant in CDE can be negative, in which case the dark energy EoS must be of quintessence type, or the coupling be positive with phantom type DE EoS. We then fix  $w_0 = -0.999$  and test the interaction constants  $\xi = -0.1, -0.01, -0.001$  and  $w_0 = -1.001$  with  $\xi = 0.001, 0.01, 0.1$ . To distinguish these two tests, we use CPDE and CQDE for phantom- and quintessence-type dark energy, respectively. The comparisons are shown in figure 1 through the modulus of the difference  $\Delta f \equiv f_{\text{anl}} - f_{\text{num}}$  divided by  $f_{\text{num}}$  (left panel), where “anl” and “num” stand for analytical and numerical computations. Over the range of the LSS data (low redshift until  $z \sim 1$ ), for a given  $\xi$ , the discrepancy grows as we approach  $z = 0$ , which is expected from the fact that  $\Omega_{\text{DE},0}$  is as big as 0.7. The discrepancy tends to decrease as  $z$  increases, but only until a certain redshift, when it can start to grow, albeit slowly. In the plot, we focus on the redshift range  $[0, 2]$ . In the  $\xi = 0.1$  case,  $f_{\text{num}}$  can become negative and the discrepancy is huge. This occurs because as  $z$  decreases,  $\frac{1-\Omega_{\text{DM}}}{\Omega_{\text{DM}}}$  increases and the second term inside the curly brackets in eq. (3.3) dominates the coefficient of  $\delta_{\text{DM}}$  and changes its sign, leading to a negative growth. The analytical parametrization  $(\Omega_{\text{DM}})^\gamma$ , on the other hand, obviously can

<sup>1</sup>The model implemented in **CAMB** had a baryonic component that could be set to account for a minimum of 0.2% of the total energy density, which should be perfectly fine as our tests showed that even the higher amount of 4% did not have a perceptible influence on the comparisons. This modified version of **CAMB** has been used in previous works [16, 41]. See ref. [42] for more details about the implementation.

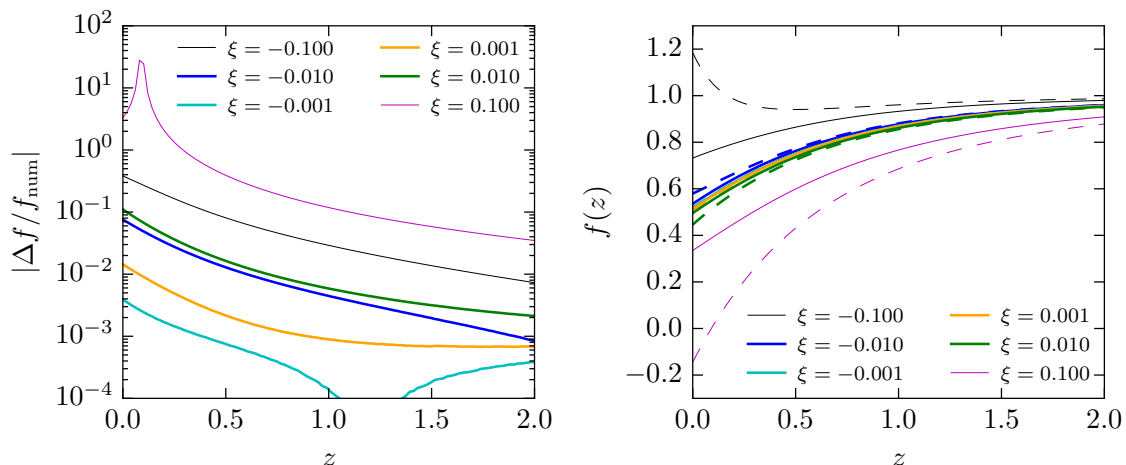


**Figure 1:** Comparison between analytical and numerical computations of  $f(z)$  for the CDE model. In the left panel, the modulus of the relative differences, in logarithmic scale; in the right panel, the dashed lines represent the numerical results for  $f(z)$ , while the solid lines show our analytical results. Values of  $|\xi|$  as big as 0.1 give large discrepancies and should be avoided. We use thin lines to represent them.

never become negative. The numerical result for  $\xi = -0.1$  shows that  $f$  grows very rapidly at small redshifts as  $z$  goes to zero, a behavior that is opposite to the other cases. This is due to a change of sign in the coefficient of  $\delta_{\text{DM}}$  (Hubble drag) in eq. (3.3). We discard the cases  $\xi = -0.1$  and  $\xi = 0.1$  as they are not well described by eq. (3.2) and restrict  $\xi$  within the interval  $[-0.01, 0]$  for the CQDE model and  $[0, 0.01]$  for the CPDE model, which allow the difference between the numerical and the analytical results to be kept below about 10% (with the other parameters fixed at reasonable values). Cusps indicating a change of sign of  $\Delta f$  are observed in the curves of  $|\Delta f/f_{\text{num}}|$  at higher redshifts (not shown). The fact that the analytical and numerical curves cross themselves instead of converging to a common plateau, with  $f_{\text{num}}$  becoming smaller than  $f_{\text{anl}}$  as  $z$  becomes larger, might indicate some contribution of a decaying mode of the perturbation, which is out of the scope of this work.

The conclusion is that the MCMC analysis can be made with high efficiency using the analytic expressions — especially useful when the computational power available is limited — derived for  $f$  in the interacting DE model, provided the parameters are restricted to the region where the discrepancy with respect to the numerical reference from CAMB is reasonably small. In the next section we present the RSD data that we use to estimate the parameters of our interacting models via MCMC.

## 4 Observational constraints

In this section we present the dataset used to constrain the parameters of our models. Because of the way those data were obtained, an adjustment to our growth rate  $f$ , calculated in a universe where DM interacts with DE, is required before comparing with  $f\sigma_8$  data. We explain in detail how the comparison must be made, then describe the statistical method employed in the analysis and discuss the results.

**Table 2:** Observed growth rate data and their respective references.

$z$	$f\sigma_8(z)$	Ref.	$z$	$f\sigma_8(z)$	Ref.
0.02	$0.360 \pm 0.040$	[45]	0.40	$0.419 \pm 0.041$	[46]
0.067	$0.423 \pm 0.055$	[47]	0.41	$0.450 \pm 0.040$	[48]
0.10	$0.37 \pm 0.13$	[49]	0.50	$0.427 \pm 0.043$	[46]
0.17	$0.510 \pm 0.060$	[36, 50]	0.57	$0.427 \pm 0.066$	[51]
0.22	$0.420 \pm 0.070$	[48]	0.60	$0.430 \pm 0.040$	[48]
0.25	$0.351 \pm 0.058$	[52]	0.60	$0.433 \pm 0.067$	[46]
0.30	$0.407 \pm 0.055$	[46]	0.77	$0.490 \pm 0.180$	[36, 53]
0.35	$0.440 \pm 0.050$	[36, 54]	0.78	$0.380 \pm 0.040$	[48]
0.37	$0.460 \pm 0.038$	[52]	0.80	$0.47 \pm 0.08$	[55]

#### 4.1 The data

One way of measuring growth of structure is through the effect of redshift-space distortions. Kaiser [43] showed that the galaxy power spectrum  $P^s$  observed in redshift space is expected to be amplified with respect to the real power spectrum  $P(k)$  by a factor that depends on the growth rate and on the cosine of the angle between the movement of the galaxies and the observation  $\mu_{kz} \equiv \frac{1}{k} \mathbf{k} \cdot \hat{\mathbf{z}}$ . The linear theory, with the plane-parallel approximation for distant observer, imposes the relation

$$P^s(\mathbf{k}) = (1 + \beta\mu_{kz}^2)^2 P(k), \quad (4.1)$$

where  $\mathbf{k}$  is the wavevector,  $k$  its modulus and  $\hat{\mathbf{z}}$  the line-of-sight direction.  $\beta$  is the so-called redshift-space distortion parameter, defined as  $\beta \equiv f(z)/b(z)$ , where  $b(z)$  is a bias parameter relating the galaxy and matter density contrasts by  $\delta_G = b\delta_M$ . The galaxy overdensity is extracted from a galaxy redshift survey. The bias can be estimated as  $\frac{\sigma_{8,G}}{\sigma_{8,M}}$ , the ratio of root-mean-square (rms) fluctuations of the two overdensity fields. Multipole analysis of the anisotropy of the redshift-space power spectrum or correlation function in the redshift survey allows the observational determination of  $\beta$ . Thus, one gets the measurement  $\beta\sigma_{8,G} = f\sigma_{8,M}$  of the growth of structure. The advantage of using  $f\sigma_8$  rather than just  $f$  to compare with model predictions is that the estimator  $\beta\sigma_{8,G}$  does not require the assumption of a bias model. Also, the determination of  $\beta$  is affected only weakly by changes in the cosmology (through the determination of distances) [36, 44].

In table 2 we list measurements of growth rate with their errors for various redshifts from different surveys like 2dF, 6dF, SDSS, BOSS and WiggleZ. Most of those data are measured using RSD and others are based on direct measurements of peculiar velocities [45, 56, 57] or galaxy luminosities [49].

##### 4.1.1 Corrections to the growth rate due to the altered continuity equation

In a standard cosmology, the coherent motion of galaxies is connected to the growth rate through the galaxy continuity equation  $\theta_G = -\mathcal{H}\beta\delta_G$ , built upon the matter continuity equation  $\theta_M = -\mathcal{H}f_M\delta_M$  with the density bias assumption  $\delta_G = b\delta_M$  and without any bias for the velocities ( $\theta_G = \theta_M$ ). Whether the RSD parameter  $\beta$  is measured from the power spectrum

or from peculiar velocities, the  $f\sigma_8$  data are based on the correspondence between  $f/b$  and the velocity divergence as established by the continuity equation. When an interacting matter component is involved, these continuity equations do not hold anymore. We will now see what quantity corresponds to the velocity divergence  $\theta_G$  in an interacting DE model.

We need to start over from the baryons and DM continuity equations in the interacting model to write a continuity equation for matter on which a continuity equation for galaxies can be based. The two matter fluids now behave differently, one coupled to the dark energy fluid and the other uncoupled. For baryons, we still have  $\dot{\delta}_B + \theta_B = 0$ . With  $Q_0^{\text{DM}} = -3\mathcal{H}\xi\bar{\rho}_{\text{DE}}$ , the DM continuity equation was obtained in section 2.2,

$$\dot{\delta}_{\text{DM}} + 3\mathcal{H}\xi\frac{\bar{\rho}_{\text{DE}}}{\bar{\rho}_{\text{DM}}}\delta_{\text{DM}} + \theta_{\text{DM}} = 0. \quad (4.2)$$

Since the matter density  $\rho_M$  is the sum of the densities  $\rho_B$  and  $\rho_{\text{DM}}$ , the matter perturbation is  $\delta_M = (\bar{\rho}_B\delta_B + \bar{\rho}_{\text{DM}}\delta_{\text{DM}})/\bar{\rho}_M$  and its time derivative is

$$\dot{\delta}_M = -3\mathcal{H}\xi\frac{\bar{\rho}_{\text{DE}}}{\bar{\rho}_M}\delta_M - \frac{\bar{\rho}_B\theta_B + \bar{\rho}_{\text{DM}}\theta_{\text{DM}}}{\bar{\rho}_M} \quad (4.3)$$

where we have also used the background evolution equations of each component from eq. (2.3). Substituting the time derivative,

$$\mathcal{H}\left(\frac{d\ln\delta_M}{d\ln a} + 3\xi\frac{\bar{\rho}_{\text{DE}}}{\bar{\rho}_M}\right)\delta_M + \frac{\bar{\rho}_B\theta_B + \bar{\rho}_{\text{DM}}\theta_{\text{DM}}}{\bar{\rho}_M} = 0. \quad (4.4)$$

Recognizing  $\theta_M$  by the term  $(\bar{\rho}_B\theta_B + \bar{\rho}_{\text{DM}}\theta_{\text{DM}})/\bar{\rho}_M$ , as usual, gives the continuity equation altered by the interaction

$$\mathcal{H}\tilde{f}_M\delta_M + \theta_M = 0, \quad (4.5)$$

where  $\tilde{f}_M \equiv f_M + 3\xi\frac{\bar{\rho}_{\text{DE}}}{\bar{\rho}_M}$  is the modified growth rate, with the usual  $f_M \equiv \frac{d\ln\delta_M}{d\ln a}$ .

We maintain the assumption that galaxies trace the matter field via  $\delta_G = b\delta_M$  and  $\theta_G = \theta_M = \theta$ , so the galaxy continuity equation is now

$$\mathcal{H}\tilde{\beta}\delta_G + \theta = 0, \quad (4.6)$$

with  $\tilde{\beta} \equiv \tilde{f}/b$ . Therefore, this modified growth rate function is the quantity that effectively corresponds to the coherent motion of galaxies if there is an interaction between DM and DE according to the CDE model considered here. Also, the RSD parameter that is effectively measured from the power spectrum is  $\tilde{\beta}$ , since the modeling of the Kaiser effect, including its nonlinear features, relies on a continuity equation like eq. (4.6)<sup>2</sup> to substitute the velocity divergence in favor of the density multiplied by the (thus modified) growth rate. The same argument applies about the treatment of nonlinear effects like the Fingers-of-God (FoG) (see, for example, refs. [58, 59]). We then just need to add the term  $3\xi\frac{\bar{\rho}_{\text{DE}}}{\bar{\rho}_M}$  to the growth rate  $f_{\text{DM}} = \Omega_{\text{DM}}^\gamma$  obtained in section 3.1 before comparing those predictions to the  $f\sigma_8$  data. In our simplified model with the matter sector composed of dark matter only, without baryonic matter, the modified growth rate is  $\tilde{f}_{\text{DM}} = f_{\text{DM}} + 3\xi\frac{1-\Omega_{\text{DM}}}{\Omega_{\text{DM}}}$ .

<sup>2</sup>Higher-order terms are generally neglected in the continuity equation.

## 4.2 The statistical method

We perform a posterior likelihood analysis with flat priors for the parameters. In order to do that, we employ our analytic formula in computing the theoretical growth, implement it in a MCMC program in python and carry out the data fitting by using a simple Metropolis algorithm [60–62]. The proposal function in the algorithm is a multivariate normal distribution centered at the current state of the Markov chain. Its covariance matrix is a diagonal matrix where each diagonal element is equal to the square of a fraction of the prior interval of its corresponding parameter, adjusted by hand to give an acceptance ratio roughly between 0.2 and 0.5 in the Metropolis algorithm [61]. The likelihoods are computed as  $\log \mathcal{L} = -\sum_{i=1}^N \log(\sigma_i \sqrt{2\pi}) - \chi^2/2$ , with

$$\chi^2 = \sum_{i=1}^N \frac{[f\sigma_8^{(\text{obs})}(z_i) - \tilde{f}\sigma_8^{(\text{th})}(z_i)]^2}{\sigma_i^2}. \quad (4.7)$$

$N$  is the number of points in the dataset,  $\sigma_i$  the errors in the measurements, “obs” stands for the observed data and “th” is our theoretical prediction by using the analytic formula on the growth. We then compute the unnormalized posterior  $P(X|D) \propto P(D|X)\pi(X)$  for the parameter-space point  $X$  given the dataset  $D$ , according to the Bayesian theorem, where  $P(D|X)$  is the likelihood  $\mathcal{L}$  and  $\pi(X)$  is the prior. Our MCMC code evolves the chains checking for convergence after each  $N_{\text{steps}}$  and keeps running until they match the convergence criteria. The starting points are chosen randomly with uniform probability within the prior ranges for each parameter. For monitoring the convergence of the chains, we implemented the multivariate extension of the method proposed by Gelman and Rubin [63, 64].

## 4.3 The results

For comparison purposes, we first constrain a simple  $\Lambda$ CDM model with the two free parameters  $\sigma_{8,0}$  and  $\Omega_{\text{DE},0}$ . Their best-fit values are used in the subsequent analysis when we compare the fitting of our models to the  $\Lambda$ CDM’s fitting with the same data in section 4.3.3. The  $f\sigma_8$  data from table 2 provide the following  $1\sigma$  confidence level (CL) for the parameters:  $\sigma_{8,0} = 0.7195_{-0.0415}^{+0.0440}$ ,  $\Omega_{\text{DE},0} = 0.6889_{-0.0691}^{+0.0606}$ , with the best-fit values  $\sigma_{8,0} = 0.7266$  and  $\Omega_{\text{DE},0} = 0.6864$  (see figure 2). The priors used were  $[0.4, 1.0]$  for both parameters and we summarize the results in table 3. The growth rate determined by the EoS parameters is

$$\Lambda\text{CDM:} \quad f(\Omega_{\text{DM}}) = (\Omega_{\text{DM}})^{0.5455+0.0073(1-\Omega_{\text{DM}})} \quad (4.8)$$

regardless of the resulting best-fit  $\sigma_{8,0}$  and  $\Omega_{\text{DE},0}$ . The growth index today is  $\gamma = 0.5505$ , up to first order in  $\Omega_{\text{DE}}$ . In the following, we present the results for the interacting DE models.

### 4.3.1 The coupled DE models

Besides  $\Omega_{\text{DE},0}$  and  $\sigma_{8,0}$ , CDE has other free parameters:  $w_0$ ,  $w_1$  and the coupling constant  $\xi$ . However, before trying to constrain all these parameters together, we first fix  $w_1 = 0$  and see if we can have a good indication of  $w_0 \neq -1$ . Not being able to constrain  $w_0$  alone in the equation of state means that we will certainly not be able to constrain  $w_0$  and  $w_1$  together. We show in figure 3 the effect of the interaction on  $\tilde{f}(z)$ ,  $\sigma_8(z)$  and on the product  $\tilde{f}\sigma_8(z)$  with  $\Omega_{\text{DE},0}$  and  $\sigma_{8,0}$  fixed at their  $\Lambda$ CDM best-fit values and with  $w_0 \rightarrow -1$ . In 3a (top panel) we can clearly see influence of the interaction on the growth rate. The constant  $\xi$  causes a shift of opposite sign to the growth rate  $f$  (not shown), but a larger shift of equal sign to the

## $\Lambda$ CDM model

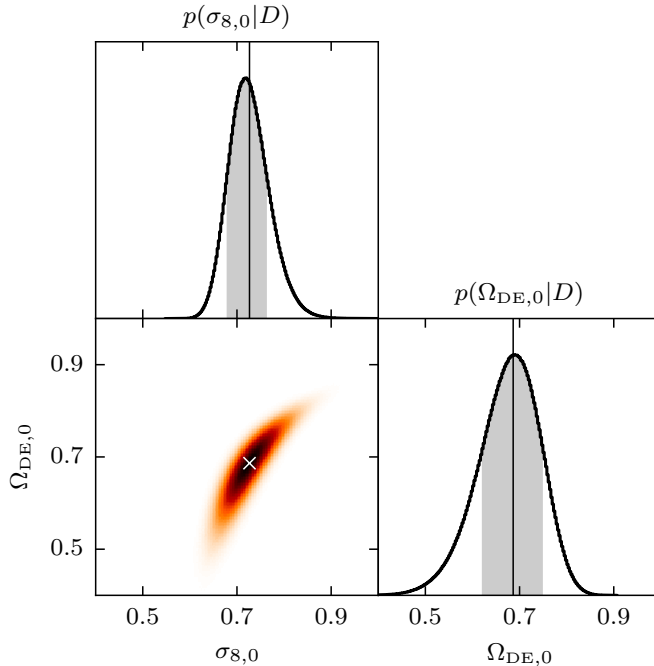


**Figure 2:** Histograms for the values of the DE density parameter and dark matter rms fluctuation today at the scale of  $8 h^{-1}$  Mpc in the  $\Lambda$ CDM model. The vertical thin lines mark the best-fit values, and the grey area under the histograms show the  $1\sigma$  CL. In the 2D histogram, the colors map the parameter space points to their unnormalized posterior values, from white (lowest values) to black (highest values), with shades of orange representing intermediate values. The white cross marks the best-fit point.

modified rate  $\tilde{f}$ , the shift getting larger as  $z$  gets closer to zero. The impact of the interaction on  $\sigma_8$  (bottom panel) is barely perceptible.

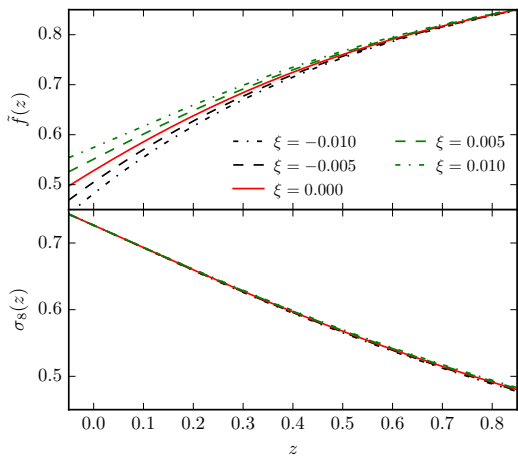
We choose the priors based on our comparison with the numerical result for  $f(z)$ , given in section 3.3. As discussed in section 2.3, in order to avoid changing the sign of the coefficient of  $\delta_{\text{DM}}$  and to keep discrepancies with respect to the numerical solutions small, values of  $\xi$  should be small, of the order  $10^{-2}$ , so we use the prior  $[0, 0.01]$  for  $\xi$  in the phantom case and  $[-0.01, 0]$  in the quintessence case.  $\Omega_{\text{DE},0}$  can be assumed any value in the interval  $(0.0, 1.0)$ .

Table 3 summarizes the priors and the fitting results and we show in figures 4 and 5a the marginalized distributions for CPDE and CQDE, respectively. We prefer to express the  $1\sigma$  CL intervals of the unconstrained parameters without reporting a central value. Because of the large uncertainties of the data, the method was not able to constrain  $w_0$  and  $\xi$  with  $f\sigma_8$  data alone, as can be seen from the histograms of the marginalized distributions. This hints the fact that such set of parameters can only be better constrained if we combine the  $f\sigma_8$  data with other kinds of observations, e.g. the CMB. The best-fit values encountered

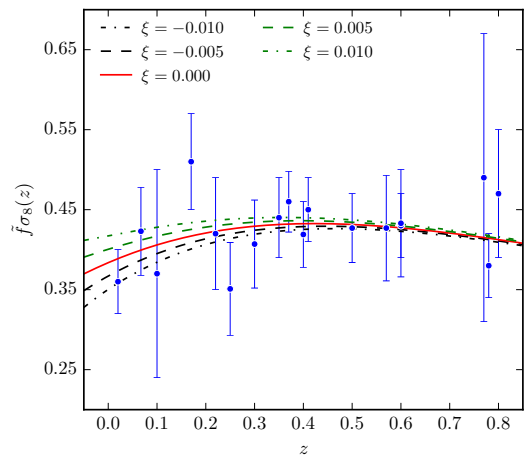


**Table 3:** Priors, best-fit values and  $1\sigma$  CL ranges for the parameters of all models. Central values are shown only for reasonably well constrained parameters.

Model	Parameter	Prior	Best-fit	$1\sigma$ CL
$\Lambda$ CDM	$\sigma_{8,0}$	[0.4, 1.0]	0.7266	$0.7195^{+0.0440}_{-0.0415}$
	$\Omega_{\text{DE},0}$	[0.4, 1.0]	0.6864	$0.6889^{+0.0606}_{-0.0691}$
CPDE	$\xi$	[0.00, 0.01]	$7.8 \times 10^{-5}$	[0.0034, 0.0100]
	$\sigma_{8,0}$	[0.2, 1.4]	0.6750	$0.6322^{+0.0473}_{-0.0293}$
	$\Omega_{\text{DE},0}$	(0.0, 1.0]	0.6712	$0.6939^{+0.0652}_{-0.0731}$
	$w_0$	[-3.0, -1.0)	-1.4173	[-2.1042, -1.0000]
CQDE	$\xi$	[-0.01, 0.00]	-0.0100	[-0.0069, 0.0000]
	$\sigma_{8,0}$	[0.2, 1.4]	0.7230	$0.7513^{+0.1262}_{-0.0598}$
	$\Omega_{\text{DE},0}$	(0.0, 1.0]	0.6533	$0.7032^{+0.0667}_{-0.0705}$
	$w_0$	(-1.0, -0.3]	-0.9977	[-1.0000, -0.5552]
$w$ CQDE	$\xi$	[-0.01, 0.00]	-0.0100	[-0.0100, -0.0031]
	$\sigma_{8,0}$	[0.2, 1.4]	0.7240	$0.7166^{+0.0412}_{-0.0386}$
	$\Omega_{\text{DE},0}$	(0.0, 1.0]	0.6546	$0.6737^{+0.0512}_{-0.0702}$



(a) Effect of  $\xi$  on  $\tilde{f}(z)$  (top) and  $\sigma_8(z)$  (bottom panel).



(b) Influence of different values of  $\xi$  on the product  $\tilde{f}\sigma_8$ .

**Figure 3:** Evolution of the growth of structures in the coupled DE model for varying values of the coupling  $\xi$ . The negative values (black lines) correspond to the CQDE model and the positive values (green lines) to the CPDE model. In both cases we use  $w_0 = -1$  for simplification, since we are interested in seeing the effect of the coupling only. The red line is the  $\Lambda$ CDM result. The data from table 2 are also plotted in (b).

## CPDE model

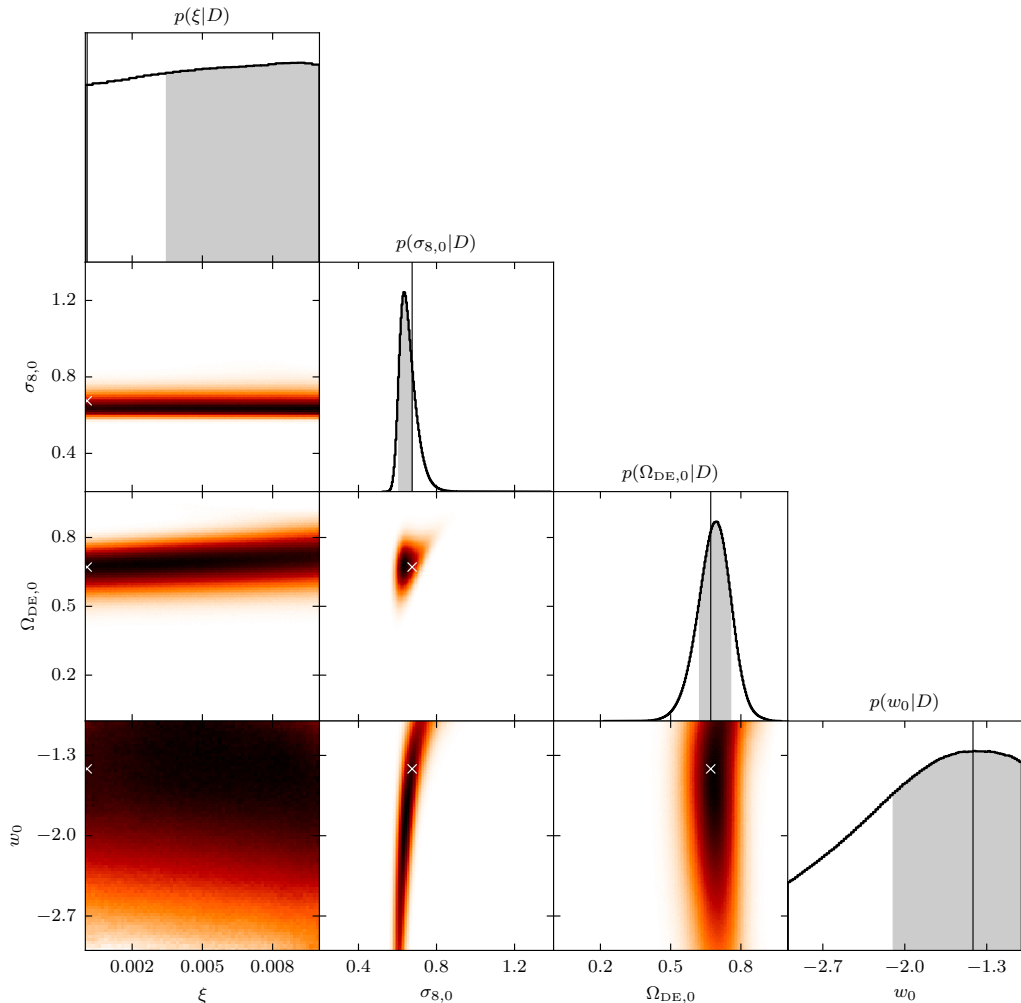


**Figure 4:** Histograms for the free parameters of CPDE. The vertical thin lines mark the best-fit values, and the grey area under the histograms show the  $1\sigma$  CL. In the 2D histograms, the colors map the parameter space points to their unnormalized posterior values, from white (lowest values) to black (highest values), with shades of orange representing intermediate values. The white crosses mark the best-fit point. Due to the large uncertainties in the RSD measurements, the data could not constrain the interaction and the EoS parameter.

lead to the growth rates

$$\text{CPDE: } f(\Omega_{\text{DM}}) = (\Omega_{\text{DM}})^{0.5371+0.0058(1-\Omega_{\text{DM}})}, \quad (4.9)$$

$$\text{CQDE: } f(\Omega_{\text{DM}}) = (\Omega_{\text{DM}})^{0.5290-0.0147(1-\Omega_{\text{DM}})}, \quad (4.10)$$

for the two models as functions of  $\Omega_{\text{DM}}$ . The best-fit  $\Omega_{\text{DE},0}$  gives, for each model, the growth index today  $\gamma = 0.5410$  and  $\gamma = 0.5194$  respectively, up to first order in the density parameter.

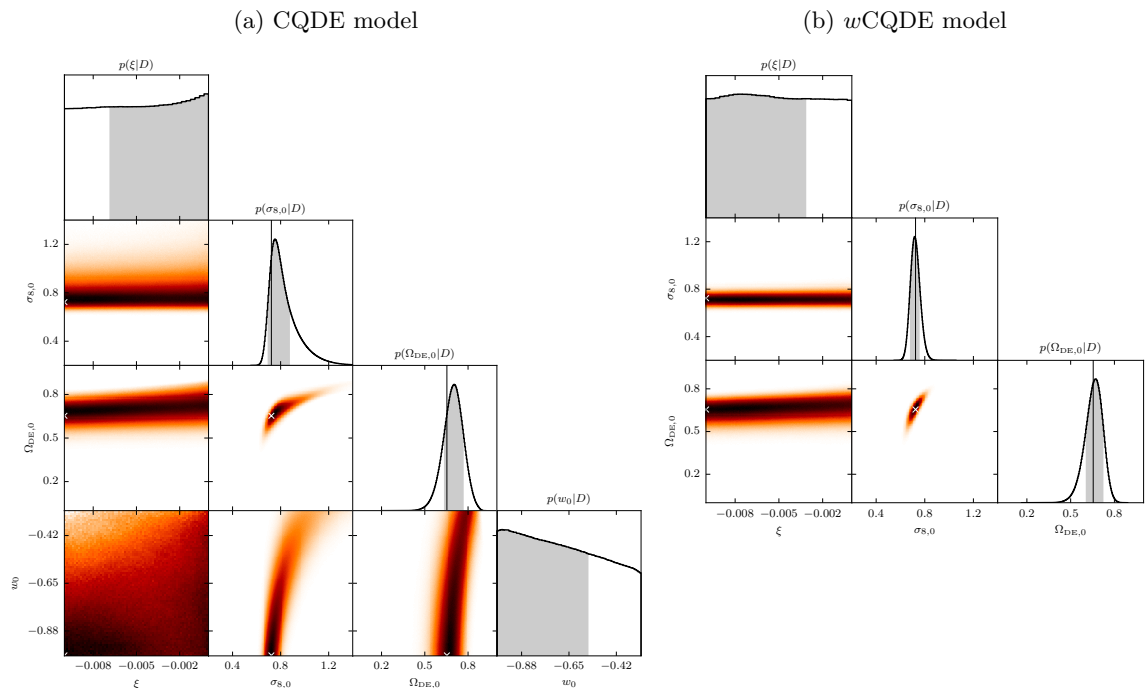


**Figure 5:** Marginalized posterior distributions for (a) CQDE and (b)  $w$ CQDE models. The vertical thin lines mark the best-fit values, while the grey areas under the histograms in the diagonal show the  $1\sigma$  CL. In the 2D histograms, the colors map the parameter space points to their unnormalized posterior values, from white (lowest values) to black (highest values), with shades of orange representing intermediate values. The white crosses mark the best-fit point. As we can see from the results of  $w$ CQDE, fixing the EoS parameter is not sufficient to constrain the interaction coupling in the already too tight prior.

### 4.3.2 On the unconstrained parameters

The models considered in our work cannot have all their parameters satisfactorily constrained due to the large uncertainties in the measurements of the large-scale structure. This difficulty motivated us to try to obtain a more conclusive determination of the interaction constant by fixing one more parameter,  $w_0$  in the equation of state. We analyze the case of CQDE with the EoS fixed in its best-fit value  $w_0 = -0.997728$ . The choice of CQDE over CPDE is because this class of models gives, according to ref. [39], the best fit to LSS data.<sup>3</sup> We then run this CQDE model with the EoS parameters fixed at  $w_0 = -0.997728$  and  $w_1 = 0$ , which we call  $w$ CQDE. The results are shown in figure 5b and in table 3. We obtained the growth rate

$$w\text{CQDE: } f(\Omega_{\text{DM}}) = (\Omega_{\text{DM}})^{0.5290 - 0.0147(1 - \Omega_{\text{DM}})}, \quad (4.11)$$

with today's value of the growth index  $\gamma = 0.5194$ . This pretty much coincides with the CQDE result, since the best-fit values of all parameters are practically identical.

We see that even when we fix the equation of state, although the region of  $1\sigma$  CL has been considerably reduced for  $\sigma_{8,0}$  and  $\Omega_{\text{DE},0}$ , the growth of structure data cannot constrain

<sup>3</sup>Which model gives the best fit to the data that we used here could be evaluated by comparing their Bayesian evidences. However, this analysis is out of the scope of this work.

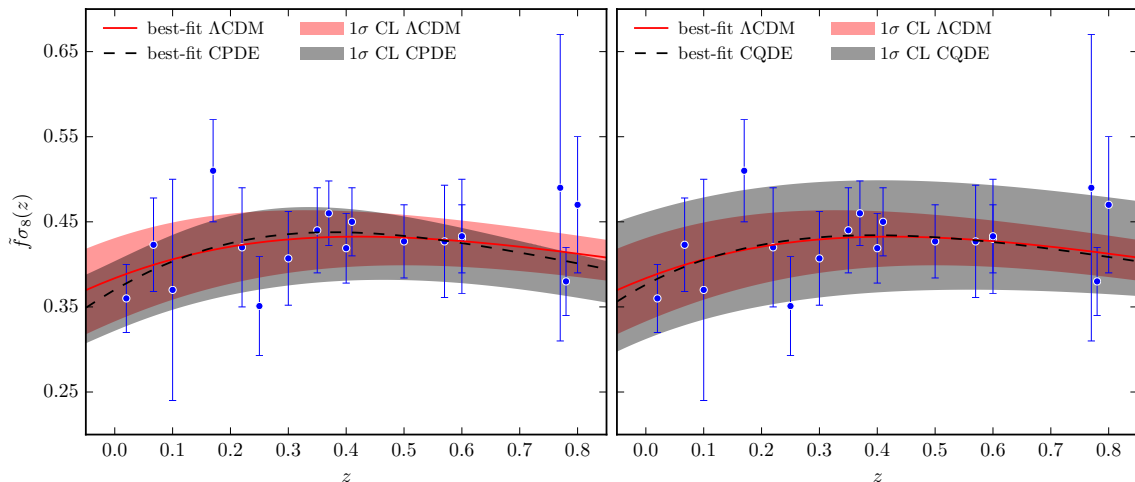


**Figure 6:** Comparisons of best-fit and  $1\sigma$ -range  $\tilde{f}\sigma_8(z)$  between CPDE and  $\Lambda$ CDM (left panel) and between CQDE and  $\Lambda$ CDM (right panel). The blue data points are listed in table 2.

very well all parameters either because the measurements are not very precise or the prior is too tight. Relaxing this prior for  $\xi$  would compromise the analysis, as the results for  $f$  would not be so reliable, as discussed in section 3.3. This last result reinforces the need of additional observables in order to get fully satisfactory constraints and make assertive conclusions about a possible detection of a DE-DM interaction.

Indeed, Yang & Xu [21] used CMB, BAO and SNe Ia in addition to  $f\sigma_8$  data to constrain an interacting  $w$ CDM model (IwCDM) which is equivalent to our CQDE model. Murgia, Gariazzo and Fornengo [65] also combined CMB temperature and polarization, gravitational lensing and supernovae data with BAO/RSD data to constrain their models MOD1 and MOD2, identical to our models CQDE and CPDE, respectively. In ref. [41], the authors combined the latest Planck CMB data, BAO, SNe Ia,  $H_0$  data and RSD to constrain several parameters of their models, which also include our models CQDE and CPDE (models I and II in ref. [41]). In all these works, the authors obtained the growth by numerically computing the perturbation equations and compared with observational datasets. Their results are consistent with our treatment by employing the analytic formula on computing the growth. All these results converge that  $f\sigma_8$  data alone cannot help to constrain well the model parameters due to the large uncertainty of the current data.

### 4.3.3 Comparing the growth in different models

In figure 6 we plot separately each of the interacting models' best-fit  $\tilde{f}\sigma_8(z)$ , together with the  $\Lambda$ CDM's best-fit over the redshift range of the data. We note that the best-fit  $\tilde{f}\sigma_8(z)$  in the CDE models is generally lower than that in  $\Lambda$ CDM, but as the redshift decreases, it surpasses  $\Lambda$ CDM around redshift  $z = 0.5$  and becomes smaller again around  $z = 0.1$ , the difference being slightly larger in the CPDE case (left panel) due to the best-fit point more distant from the  $\Lambda$ CDM best-fit.

The discrepancies between the models become more apparent when we look at the  $1\sigma$  ranges and at the functions  $\tilde{f}(z)$ ,  $\sigma_8(z)$  and  $\gamma(z)$  separately. In order to do that, we perform

**Table 4:** Centralized  $1\sigma$  CL intervals of the free parameters in  $\Lambda$ CDM and interacting models for the linear error propagation.

Parameter	$\Lambda$ CDM	CPDE	CQDE
$\xi \pm \Delta\xi$	0.0	$0.0067 \pm 0.0033$	$-0.0034 \pm 0.0034$
$\sigma_{8,0} \pm \Delta\sigma_{8,0}$	$0.7209 \pm 0.0426$	$0.6412 \pm 0.0383$	$0.7845 \pm 0.0930$
$\Omega_{\text{DE},0} \pm \Delta\Omega_{\text{DE},0}$	$0.6846 \pm 0.0649$	$0.6900 \pm 0.0692$	$0.7013 \pm 0.0686$
$w_0 \pm \Delta w_0$	-1.0	$-1.5521 \pm 0.5521$	$-0.7776 \pm 0.2224$

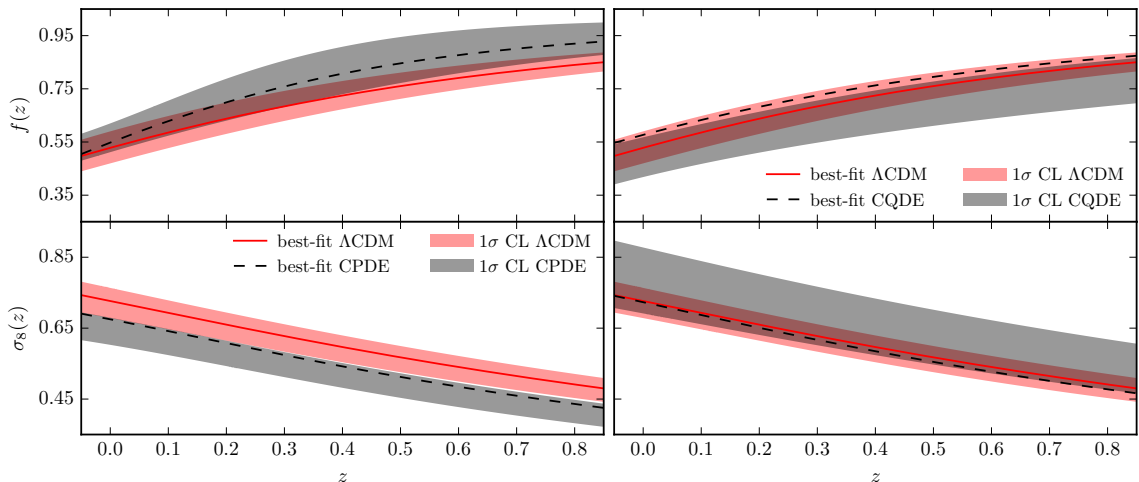


**Figure 7:** Comparisons of best-fit and  $1\sigma$ -range  $f(z)$  (upper panels) and  $\sigma_8(z)$  (lower panels) between CPDE and  $\Lambda$ CDM (left panels) and between CQDE and  $\Lambda$ CDM (right panels).

linear error propagation on the fitted parameters. We simplify the task by centralizing the  $1\sigma$  CL intervals, getting the values listed in table 4, then propagate the errors through eqs. (3.11), (3.2), (3.20) and (3.23).

Although CQDE’s best-fit is closer to  $\Lambda$ CDM than CPDE’s best-fit, CQDE presents a wider  $1\sigma$  range, encompassing the entire  $\Lambda$ CDM  $1\sigma$  range (see figure 6). CPDE’s  $1\sigma$  range is about as wide as  $\Lambda$ CDM’s. The three models are overall consistent within  $1\sigma$  CL.

In figure 7 we analyze the unmodified  $f(z)$  and  $\sigma_8(z)$  separately. Faster growth rate means less dark matter in the past and explains the corresponding lower amplitudes  $\sigma_8$  for CPDE, which presents higher  $f(z)$  compared to  $\Lambda$ CDM. The opposite happens in CQDE. The differences between the interacting models and  $\Lambda$ CDM appear to enhance as  $z$  increases. The interacting models’  $1\sigma$  ranges are consistent with  $\Lambda$ CDM except for CPDE’s  $1\sigma$ -range  $\sigma_8$ , which is only marginally consistent with  $\Lambda$ CDM at low redshifts.

The  $1\sigma$  range interval of  $\gamma(z)$  in  $\Lambda$ CDM (see figure 8) is very tight because the only uncertainty involved is in the  $\Omega_{\text{DE},0}$  parameter, which is well constrained. The best-fit growth index is lower than  $\Lambda$ CDM’s best-fit in the two CDE models, falling closer to  $\Lambda$ CDM in the CPDE case and outside its own  $1\sigma$  range in the CQDE case. However, their  $1\sigma$  ranges are still consistent with  $\Lambda$ CDM in the redshift interval we are considering.

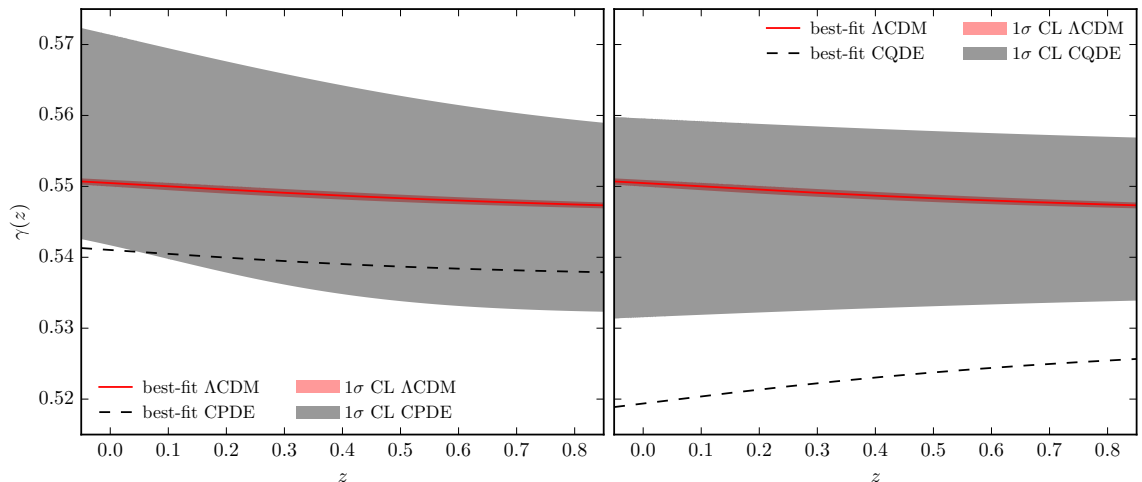


**Figure 8:** Comparisons of best-fit and  $1\sigma$ -range  $\gamma(z)$  between CPDE and  $\Lambda$ CDM (left panel) and between CQDE and  $\Lambda$ CDM (right panel).

## 5 Conclusions

In this work we have obtained the linear evolution equations for the perturbations of the dark matter fluid in cosmology with interaction in the dark sectors. We then rewrote those equations in terms of the growth rate, did the Taylor expansion around  $\Omega_{\text{DE}} = 0$  and succeeded in deriving an analytic approximation for the growth index  $\gamma$  when the interaction is proportional to  $\rho_{\text{DE}}$ . The solution (3.11) depends on the parameters of the dynamical DE equation of state and on the interaction coupling constant. The obtained analytic result for the growth index allows us to have the evolution of the growth of structures once the parameters of the coupled model are determined. Comparing with numerical calculations, we have proved that our analytic treatment works precisely within a region of the parameter space. The benefit of the analytic expression is that the influence of the coupling between dark sectors can be reflected clearly in the growth, which can help to distinguish from the models without interaction between DM and DE. Furthermore, using the analytic growth formula, we can potentially reduce the computation time and confront our model to the observations more efficiently. In fact, in our analyses we were able to achieve convergence typically four orders of magnitude better, using a rather modest workstation, than in similar MCMC analyses made with `CosmoMC` [66] and full numerical calculations in `CAMB`, running on a dedicated computer cluster, in comparable amounts of time. We have done the data fitting by confronting our model to the RSD observations.

On the other hand, we noticed that our analytic treatment is not generally effective. For example, when the interaction between dark sectors is proportional to the energy density of DM, the polynomial equation in  $\Omega_{\text{DE}}$  forces the coupling to be always zero (see appendix A for details). This problem can probably be solved if we can adopt a different parametrization of the growth rate. However, the generalization is not trivial and we leave it for further careful investigation in the future.

Although theoretically we can predict the differences caused by the interaction between dark sectors in the growth of structures from the growth in other models, tight constraints on the model parameters, such as the DE EoS and the coupling, by using  $f\sigma_8$  data exclusively

are difficult to be obtained. This is mainly because of the low quality of the data at this moment. We expect that the situation can be improved soon in the next years with the advent of a new generation of powerful telescopes, e.g. the SKA [67], BINGO [68, 69], Euclid [70] and J-PAS [71] projects.

## A The case of an interaction proportional to the DM density

We have also analyzed the case of an interaction proportional to the DM density,  $Q_0^{\text{DM}} = -3\mathcal{H}\xi\rho_{\text{DM}}$ . We set the perturbed spatial part  $\delta Q_i^{\text{DM}} = 0$ . The background evolution is given by  $\dot{\rho}_{\text{DM}} + 3\mathcal{H}\bar{\rho}_{\text{DM}} = 3\mathcal{H}\xi\bar{\rho}_{\text{DM}}$ . The perturbation equations (2.8) with  $\frac{\dot{Q}_0^{\text{DM}}}{\rho_{\text{DM}}} = \frac{\delta Q_0^{\text{DM}}}{\rho_{\text{DM}}\delta_{\text{DM}}} = -3\mathcal{H}\xi$  are

$$\dot{\delta}_{\text{DM}} + \theta_{\text{DM}} = 0 \quad (\text{A.1a})$$

$$\dot{\theta}_{\text{DM}} + (1 + 3\xi)\mathcal{H}\theta + \frac{3}{2}\mathcal{H}^2\Omega_{\text{DM}}\delta_{\text{DM}} = 0 \quad (\text{A.1b})$$

and give

$$\ddot{\delta}_{\text{DM}} + (1 + 3\xi)\mathcal{H}\dot{\delta}_{\text{DM}} - \frac{3}{2}\mathcal{H}^2\Omega_{\text{DM}}\delta_{\text{DM}} = 0. \quad (\text{A.2})$$

The functional form of this equation is even simpler than the CDE case of section 3.1 with respect to the standard evolution, with only one extra term proportional to  $\xi$  in the coefficient of  $\dot{\delta}_{\text{DM}}$ .

In terms of  $f = \Omega_{\text{DM}}^\gamma$ , with  $\frac{d\Omega_{\text{DM}}}{d\ln a} = 3\Omega_{\text{DM}}[\xi + w_{\text{DE}}(1 - \Omega_{\text{DM}})]$ , the growth rate evolution equation is

$$3[w_{\text{DE}}(1 - \Omega_{\text{DM}}) + \xi]\frac{\Omega_{\text{DM}}}{f}\frac{df}{d\Omega_{\text{DM}}} + f + \frac{1}{2} - \frac{3}{2}w_{\text{DE}}(1 - \Omega_{\text{DM}}) + 3\xi - \frac{3}{2}\frac{\Omega_{\text{DM}}}{f} = 0, \quad (\text{A.3})$$

which expanded in  $\Omega_{\text{DE}}$  for  $f = (\Omega_{\text{DM}})^{\gamma_0 + \gamma_1\Omega_{\text{DE}} + \dots}$  gives the polynomial equation

$$\begin{aligned} & 3\xi(1 + \gamma_0) + \frac{1}{2}[3(1 - w_0) - (5 - 6w_0)\gamma_0 + 12\xi\gamma_1]\Omega_{\text{DE}} + \\ & + \frac{1}{4}[-\gamma_0^2 + 36\xi\gamma_2 + 2\gamma_1(12w_0 - 5 - 3\xi) + (1 + 12w_1)\gamma_0 - 6w_1]\Omega_{\text{DE}}^2 + \mathcal{O}(\Omega_{\text{DE}}^3) = 0. \end{aligned} \quad (\text{A.4})$$

Unlike eq. (3.10), this now has a zero-th order part that does not vanish automatically and regardless of the interaction or other parameters as in the other model). In order for eq. (A.4) to hold,  $3\xi(1 + \gamma_0) = 0$  must be satisfied. This implies  $\xi = 0$ , recovering the non-interacting results for  $\gamma$  from the higher order terms, or  $\gamma_0 = -1$  and  $\gamma_1 = \frac{9w_0 - 8}{12\xi}$  (with  $\xi \neq 0$ ) from the first-order coefficient, which does not seem to fit the observed growth unless perhaps with a fine tuning of the parameters. Also, note that this solution implies a non-smooth transition to zero interaction. Although numerically the growth rate in this model can still be, to some degree, well approximated by the power law  $\Omega_{\text{DM}}^\gamma$  form, as claimed in ref. [35], analytically we can see that this form is not appropriate for a non-zero coupling in the interaction term that is proportional to  $\rho_{\text{DM}}$ .

## Acknowledgments

This work is supported by CAPES, CNPq, FAPESP (Nos. 2011/18729-1, 2013/10242-1, 2013/26496-2), National Basic Research Program of China (973 Program 2013CB834900) and National Natural Science Foundation of China.

## References

- [1] **Supernova Search Team** Collaboration, A. G. Riess et al., *Observational Evidence from Supernovae for an Accelerating Universe and a Cosmological Constant*, *Astron. J.* **116** (1998) 1009, [[astro-ph/9805201](#)].
- [2] **Supernova Cosmology Project** Collaboration, S. Perlmutter et al., *Measurements of  $\Omega$  and  $\Lambda$  from 42 High-Redshift Supernovae*, *Astrophys. J.* **517** (1999) 565, [[astro-ph/9812133](#)].
- [3] F. Zwicky, *Republication of: The redshift of extragalactic nebulae*, *Gen. Rel. Grav.* **41** (2009) 207.
- [4] F. Zwicky, *On the Masses of Nebulae and of Clusters of Nebulae*, *Astrophys. J.* **86** (1937) 217.
- [5] L. Amendola, *Coupled quintessence*, *Phys. Rev. D* **62** (2000) 043511, [[astro-ph/9908023](#)].
- [6] S. del Campo, R. Herrera, G. Olivares, and D. Pavón, *Interacting models of soft coincidence*, *Phys. Rev. D* **74** (2006) 023501, [[astro-ph/0606520](#)].
- [7] V. Poitras, *Can the coincidence problem be solved by a cosmological model of coupled dark energy and dark matter?*, *Gen. Rel. Grav.* **46** (2014) 1732, [[arXiv:1307.6172](#)].
- [8] J.-H. He and B. Wang, *Effects of the interaction between dark energy and dark matter on cosmological parameters*, *JCAP* **06** (2008) 010, [[arXiv:0801.4233](#)].
- [9] E. Abdalla, L. R. Abramo, L. Sodré Jr., and B. Wang, *Signature of the interaction between dark energy and dark matter in galaxy clusters*, *Phys. Lett. B* **673** (2009) 107, [[arXiv:0710.1198](#)].
- [10] E. Abdalla, L. R. Abramo, and J. C. de Souza, *Signature of the interaction between dark energy and dark matter in observations*, *Phys. Rev. D* **82** (2010) 023508, [[arXiv:0910.5236](#)].
- [11] J.-H. He, B. Wang, and E. Abdalla, *Testing the interaction between dark energy and dark matter via the latest observations*, *Phys. Rev. D* **83** (2011) 063515, [[arXiv:1012.3904](#)].
- [12] S. Cao, N. Liang, and Z.-H. Zhu, *Testing the phenomenological interacting dark energy with observational  $H(z)$  data*, *Mon. Not. Roy. Astron. Soc.* **416** (2011) 1099, [[arXiv:1012.4879](#)].
- [13] F. C. Solano and U. Nucamendi, *Reconstruction of the interaction term between dark matter and dark energy using SNe Ia*, *JCAP* **04** (2012) 011, [[arXiv:1109.1303](#)].
- [14] Z. Li, *Interacting dark energy: a generalized scenario and observational constraints*, *Eur. Phys. J. C* **73** (2013).
- [15] S. Cao and N. Liang, *Interaction between dark energy and dark matter: observational constraints from OHD, BAO, CMB and SNe Ia*, *Int. J. Mod. Phys. D* **22** (2013) 1350082, [[arXiv:1105.6274](#)].
- [16] A. A. Costa, X.-D. Xu, B. Wang, E. G. M. Ferreira, and E. Abdalla, *Testing the interaction between dark energy and dark matter with Planck data*, *Phys. Rev. D* **89** (2014) 103531, [[arXiv:1311.7380](#)].
- [17] A. A. Costa, L. C. Olivari, and E. Abdalla, *Quintessence with Yukawa interaction*, *Phys. Rev. D* **92** (2015) 103501, [[arXiv:1411.3660](#)].
- [18] M. Le Delliou, R. Marcondes, G. Lima Neto, and E. Abdalla, *Non-virialized clusters for detection of dark energy–dark matter interaction*, *Mon. Not. Roy. Astron. Soc.* **453** (2015) 2, [[arXiv:1411.5863](#)].
- [19] B. Wang, E. Abdalla, F. Atrio-Barandela, and D. Pavón, *Dark matter and dark energy interactions: theoretical challenges, cosmological implications and observational signatures*, *Rep. Prog. Phys.* **79** (2016), no. 9 096901, [[arXiv:1603.08299](#)].
- [20] S. Tsujikawa, A. D. Felice, and J. Alcaniz, *Testing for dynamical dark energy models with redshift-space distortions*, *JCAP* **01** (2013) 030, [[arXiv:1210.4239](#)].



- [21] W. Yang and L. Xu, *Cosmological constraints on interacting dark energy with redshift-space distortion after Planck data*, *Phys. Rev. D* **89** (2014) 083517, [[arXiv:1401.1286](#)].
- [22] Y.-H. Li, J.-F. Zhang, and X. Zhang, *Exploring the full parameter space for an interacting dark energy model with recent observations including redshift-space distortions: Application of the parametrized post-Friedmann approach*, *Phys. Rev. D* **90** (2014) 123007, [[arXiv:1409.7205](#)].
- [23] M. G. Richarte and L. Xu, *Exploring a new interaction between dark matter and dark energy using the growth rate of structure*, *ArXiv e-prints* (2015) [[arXiv:1506.02518](#)].
- [24] Y.-H. Li, J.-F. Zhang, and X. Zhang, *Testing models of vacuum energy interacting with cold dark matter*, *Phys. Rev. D* **93** (2016) 023002, [[arXiv:1506.06349](#)].
- [25] P. J. E. Peebles, *The Large-Scale Structure of the Universe*. Princeton University Press, 1980.
- [26] A. P. Lightman and P. L. Schechter, *The  $\Omega$  dependence of peculiar velocities induced by spherical density perturbations*, *Astrophys. J., Suppl. Ser.* **74** (1990) 831.
- [27] L. Wang and P. J. Steinhardt, *Cluster Abundance Constraints for Cosmological Models with a Time-varying, Spatially Inhomogeneous Energy Component with Negative Pressure*, *Astrophys. J.* **508** (1998) 483, [[astro-ph/9804015](#)].
- [28] Y. Gong, M. Ishak, and A. Wang, *Growth factor parametrization in curved space*, *Phys. Rev. D* **80** (2009) 023002, [[arXiv:0903.0001](#)].
- [29] E. V. Linder and R. N. Cahn, *Parameterized beyond-Einstein growth*, *Astropart. Phys.* **28** (2007) 481, [[astro-ph/0701317](#)].
- [30] Y. Gong, *Growth factor parametrization and modified gravity*, *Phys. Rev. D* **78** (2008) 123010, [[arXiv:0808.1316](#)].
- [31] R. Gannouji and D. Polarski, *The growth of matter perturbations in some scalar-tensor DE models*, *JCAP* **05** (2008) 018, [[arXiv:0802.4196](#)].
- [32] J. Dossett, M. Ishak, J. Moldenhauer, Y. Gong, and A. Wang, *Constraints on growth index parameters from current and future observations*, *JCAP* **04** (2010) 022, [[arXiv:1004.3086](#)].
- [33] G. R. Farrar and P. Peebles, *Interacting Dark Matter and Dark Energy*, *Astrophys. J.* **604** (2004) 1, [[astro-ph/0307316](#)].
- [34] D. G. A. Duniya, D. Bertacca, and R. Maartens, *Clustering of quintessence on horizon scales and its imprint on HI intensity mapping*, *JCAP* **10** (2013) 015, [[arXiv:1305.4509](#)].
- [35] E. V. Linder, *Cosmic growth history and expansion history*, *Phys. Rev. D* **72** (2005) 043529, [[astro-ph/0507263](#)].
- [36] Y.-S. Song and W. J. Percival, *Reconstructing the history of structure formation using redshift distortions*, *JCAP* **10** (2009) 004, [[arXiv:0807.0810](#)].
- [37] J. Väliiviita, E. Majerotto, and R. Maartens, *Large-scale instability in interacting dark energy and dark matter fluids*, *JCAP* **07** (2008) 020, [[arXiv:0804.0232](#)].
- [38] J.-H. He, B. Wang, and E. Abdalla, *Stability of the curvature perturbation in dark sectors' mutual interacting models*, *Phys. Lett. B* **671** (2009) 139, [[arXiv:0807.3471](#)].
- [39] M. Gavela, D. Hernandez, L. L. Honorez, O. Mena, and S. Rigolin, *Dark coupling*, *JCAP* **07** (2009) 034, [[arXiv:0901.1611](#)].
- [40] A. Lewis, A. Challinor, and A. Lasenby, *Efficient computation of CMB anisotropies in closed FRW models*, *Astrophys. J.* **538** (2000) 473, [[astro-ph/9911177](#)].
- [41] A. A. Costa, X.-D. Xu, B. Wang, and E. Abdalla, *Constraints on interacting dark energy models from Planck 2015 and redshift-space distortion data*, *ArXiv e-prints* (2016) [[arXiv:1605.04138](#)].

- [42] A. A. Costa, *Observational Constraints on Models with an Interaction between Dark Energy and Dark Matter*. PhD thesis, Institute of Physics, University of São Paulo, 2014.
- [43] N. Kaiser, *Clustering in real space and in redshift space*, *Mon. Not. Roy. Astron. Soc.* **227** (1987) 1.
- [44] S. Basilakos, S. Nesseris, and L. Perivolaropoulos, *Observational constraints on viable  $f(R)$  parametrizations with geometrical and dynamical probes*, *Phys. Rev. D* **87** (2013) 123529, [[arXiv:1302.6051](#)].
- [45] M. J. Hudson and S. J. Turnbull, *The Growth Rate of Cosmic Structure from Peculiar Velocities at Low and High Redshifts*, *Astrophys. J. Let.* **751** (2012) L30, [[arXiv:1203.4814](#)].
- [46] **SDSS** Collaboration, R. Tojeiro et al., *The clustering of galaxies in the SDSS-III Baryon Oscillation Spectroscopic Survey: measuring structure growth using passive galaxies*, *Mon. Not. Roy. Astron. Soc.* **424** (2012) 2339, [[arXiv:1203.6565](#)].
- [47] F. Beutler, C. Blake, M. Colless, D. H. Jones, L. Staveley-Smith, G. B. Poole, L. Campbell, Q. Parker, W. Saunders, and F. Watson, *The 6dF Galaxy Survey:  $z \approx 0$  measurements of the growth rate and  $\sigma_8$* , *Mon. Not. Roy. Astron. Soc.* **423** (2012) 3430, [[arXiv:1204.4725](#)].
- [48] **WiggleZ** Collaboration, C. Blake et al., *The WiggleZ Dark Energy Survey: the growth rate of cosmic structure since redshift  $z = 0.9$* , *Mon. Not. Roy. Astron. Soc.* **415** (2011) 2876, [[arXiv:1104.2948](#)].
- [49] M. Feix, A. Nusser, and E. Branchini, *Growth Rate of Cosmological Perturbations at  $z \sim 0.1$  from a New Observational Test*, *Phys. Rev. Let.* **115** (2015) 011301, [[arXiv:1503.05945](#)].
- [50] **The 2dFGRS Team** Collaboration, W. J. Percival et al., *The 2dF Galaxy Redshift Survey: spherical harmonics analysis of fluctuations in the final catalogue*, *Mon. Not. Roy. Astron. Soc.* **353** (2004) 1201, [[astro-ph/0406513](#)].
- [51] **SDSS** Collaboration, B. A. Reid et al., *The clustering of galaxies in the SDSS-III Baryon Oscillation Spectroscopic Survey: measurements of the growth of structure and expansion rate at  $z = 0.57$  from anisotropic clustering*, *Mon. Not. Roy. Astron. Soc.* **426** (2012) 2719, [[arXiv:1203.6641](#)].
- [52] L. Samushia, W. Percival, and A. Raccanelli, *Interpreting large-scale redshift-space distortion measurements*, *Mon. Not. Roy. Astron. Soc.* **420** (2012) 2102, [[arXiv:1102.1014](#)].
- [53] L. Guzzo, M. Pierleoni, B. Meneux, E. Branchini, O. L. Fevre, et al., *A test of the nature of cosmic acceleration using galaxy redshift distortions*, *Nature* **451** (2008) 541, [[arXiv:0802.1944](#)].
- [54] **SDSS** Collaboration, M. Tegmark et al., *Cosmological constraints from the SDSS luminous red galaxies*, *Phys. Rev. D* **74** (2006) 123507, [[astro-ph/0608632](#)].
- [55] **VIPERS** Collaboration, S. de la Torre et al., *The VIMOS Public Extragalactic Redshift Survey (VIPERS) – Galaxy clustering and redshift-space distortions at  $z = 0.8$  in the first data release*, *Astron. Astrophys.* **557** (2013) A54, [[arXiv:1303.2622](#)].
- [56] S. J. Turnbull, M. J. Hudson, H. A. Feldman, M. Hicken, R. P. Kirshner, and R. Watkins, *Cosmic flows in the nearby universe from Type Ia supernovae*, *Mon. Not. Roy. Astron. Soc.* **420** (2012) 447, [[arXiv:1111.0631](#)].
- [57] M. Davis, A. Nusser, K. L. Masters, C. Springob, J. P. Huchra, and G. Lemson, *Local gravity versus local velocity: solutions for  $\beta$  and non-linear bias*, *Mon. Not. Roy. Astron. Soc.* **413** (2011) 2906, [[arXiv:1011.3114](#)].
- [58] M. Oh and Y.-S. Song, *Measuring neutrino mass imprinted on the anisotropic galaxy clustering*, *ArXiv e-prints* (2016) [[arXiv:1607.01074](#)].

- [59] A. Taruya, T. Nishimichi, and S. Saito, *Baryon acoustic oscillations in 2D: Modeling redshift-space power spectrum from perturbation theory*, *Phys. Rev. D* **82** (2010) 063522.
- [60] C. Geyer, *Introduction to Markov Chain Monte Carlo*, in *Chapman & Hall/CRC Handbooks of Modern Statistical Methods*. Informa UK Limited, 2011.
- [61] D. Foreman-Mackey, D. Hogg, D. Lang, and J. Goodman, *emcee: The MCMC Hammer*, *Publ. Astron. Soc. Pac.* **125** (2013) 306, [[arXiv:1202.3665](#)].
- [62] A. Heavens, *Statistical techniques in cosmology*, *ArXiv e-prints* (2010) [[arXiv:0906.0664](#)].
- [63] A. Gelman and D. B. Rubin, *Inference from Iterative Simulation Using Multiple Sequences*, *Stat. Sci.* **7** (1992) 457.
- [64] S. P. Brooks and A. Gelman, *General Methods for Monitoring Convergence of Iterative Simulations*, *J. Comput. Graph. Stat.* **7** (1998) 434.
- [65] R. Murgia, S. Gariazzo, and N. Fornengo, *Constraints on the coupling between dark energy and dark matter from CMB data*, *JCAP* **04** (2016) 014, [[arXiv:1602.01765](#)].
- [66] A. Lewis and S. Bridle, *Cosmological parameters from CMB and other data: A Monte Carlo approach*, *Phys. Rev. D* **66** (2002) 103511, [[astro-ph/0205436](#)].
- [67] P. E. Dewdney, P. J. Hall, R. T. Schilizzi, and T. J. L. W. Lazio, *The Square Kilometre Array*, *Proc. IEEE* **97** (2009) 1482.
- [68] R. A. Battye, M. L. Brown, I. W. A. Browne, R. J. Davis, P. Dewdney, C. Dickinson, G. Heron, B. Maffei, A. Pourtsidou, and P. N. Wilkinson, *BINGO: a single dish approach to 21cm intensity mapping*, *ArXiv e-prints* (2012) [[arXiv:1209.1041](#)].
- [69] C. Dickinson, *BINGO - A novel method to detect BAOs using a total-power radio telescope*, *ArXiv e-prints* (2014) [[arXiv:1405.7936](#)].
- [70] L. Amendola and Euclid Theory Working Group, *Cosmology and fundamental physics with the euclid satellite*, *Living Reviews in Relativity* **16** (2013), no. 6 [[arXiv:1206.1225](#)].
- [71] N. Benitez et al., *J-PAS: The Javalambre-Physics of the Accelerated Universe Astrophysical Survey*, *ArXiv e-prints* (2014) [[arXiv:1403.5237](#)].